CrossMark

Applicability of rat precision-cut lung slices in evaluating nanomaterial cytotoxicity, apoptosis, oxidative stress, and inflammation

Ursula G. Sauer [a,1], Sandra Vogel [b,c,1], Alexandra Aumann [b], Annemarie Hess [b], Susanne N. Kolle [b], Lan Ma-Hock [b], Wendel Wohlleben [b,d], Martina Dammann [b], Volker Strauss [b], Silke Treumann [b], Sibylle Gröters [b], Karin Wiench [e], Bennard van Ravenzwaay [b], Robert Landsiedel [b,*]

[a] Scientific Consultancy — Animal Welfare, Neubiberg, Germany
[b] Experimental Toxicology and Ecology, BASF SE, Ludwigshafen, Germany
[c] Product Stewardship Water Solutions, BASF SE, Ludwigshafen, Germany
[d] Material Physics, BASF SE, Ludwigshafen, Germany
[e] Product Safety, BASF SE, Ludwigshafen, Germany

ARTICLE INFO

ABSTRACT

The applicability of rat precision-cut lung slices (PCLuS) in detecting nanomaterial (NM) toxicity to the respiratory tract was investigated evaluating sixteen OECD reference NMs (TiO$_2$, ZnO, CeO$_2$, SiO$_2$, Ag, multi-walled carbon nanotubes (MWCNTs)). Upon 24-hour test substance exposure, the PCLuS system was able to detect early events of NM toxicity: total protein, reduction in mitochondrial activity, caspase-3/-7 activation, glutathione depletion/increase, cytokine induction, and histopathological evaluation. Ion shedding NMS (ZnO and Ag) induced severe tissue destruction detected by the loss of total protein. Two anatase TiO$_2$ NMs, CeO$_2$ NMs, and two MWCNT caused significant (determined by trend analysis) cytotoxicity in the WST-1 assay. At non-cytotoxic concentrations, different TiO$_2$ NMs and one MWCNT increased GSH levels, presumably a defense response to reactive oxygen species, and these substances further induced a variety of cytokines. One of the SiO$_2$ NMs increased caspase-3/-7 activities at non-cytotoxic levels, and one rutile TiO$_2$ only induced cytokines. Investigating these effects is, however, not sufficient to predict apical effects found in vivo. Reproducibility of test substance measurements was not fully satisfactory, especially in the GSH and cytokine assays. Effects were frequently observed in negative controls pointing to tissue slice vulnerability even though prepared and handled with utmost care. Comparisons of the effects observed in the PCLuS to in vivo effects reveal some concordances for the metal oxide NMs, but less so for the MWCNT. The highest effective dosages, however, exceeded those reported for rat short-term inhalation studies. To become applicable for NM testing, the PCLuS system requires test protocol optimization.

© 2013 The Authors. Published by Elsevier Inc. Open access under CC BY license.

Introduction

have advanced. NMs have been defined as "natural, incidental or manufactured material[s] containing particles, in an unbound state or as an aggregate or as an agglomerate and where, for 50% or more of the particles in the number size distribution, one or more external dimensions is in the size range 1 nm–100 nm" (Anon, 2011). The

OECD's Working Party on Manufactured Nanomaterials (WPMN) has launched a *Sponsorship Programme for the Testing of Manufactured* [...]sh [...]or [...]ls (OECD, 2008, 2010). One aim of the WPMN is to collect relevant data for the safety assessment of a representative set of NMs and to establish the role of alternative methods to animal testing in nanotoxicology (OECD, 2008).

As regards exposure to NMs, inhalation is recognized as a main route of uptake, especially in the occupational context, but also for consumers (Aitken et al., 2011; Klein et al., 2012). The WPMN has proposed a short-term rat inhalation study (STIS) as a suitable reduction and refinement alternative to obtain information on early key elements of pathogenesis, as well as on the persistence, progression and/or regression of effects, while also addressing organ burden in the lung and potential transloca-tion to other tissues (Klein et al., 2012). Additionally, intratracheal instillation studies have been applied for NM testing. However, the

biological relevance of applying substances by this form of administration has been questioned (Landsiedel et al., 2012). Although animal numbers and exposure durations are reduced in these two in vivo methods as compared to the acute inhalation toxicity study described in OECD Test Guideline 403 (OECD, 2009), they both still require the use and euthanasia of animals.

A replacement method to determine nanomaterial short-term inhalation toxicity remains to be developed. Nanomaterials have been applied in a vast amount of different cell culture systems consisting of one or more cell types — of pulmonary or other origin, using human or animal primary cells or cell lines, and a variety of different endpoint detection methods (Hackenberg et al., 2011; Kroll et al., 2011; Stone et al., 2009). Cells have been cultured in suspension or at the air–liquid interface (Rothen-Rutishauser et al., 2005). The results obtained in such in vitro test methods have not been consistent, and standardized in vitro test methods to determine early cellular effects upon NM exposure remain to be developed (Gasser et al., 2012; Nel et al., 2013a,b). Consequently, the relevance of in vitro test results in predicting NM effects in vivo is a matter of controversy, not least because cell culture systems lack the structural identity of the pulmonary tissue (Hirsch et al., 2011; Nel et al., 2013a).

Against this background it was the goal of the current study to investigate the applicability of rat precision-cut lung slices (PCLuS) as an ex vivo test method to determine the respiratory effects of NMs. Whereas a pre-validation study investigating the suitability of PCLuS in predicting short-term respiratory toxicity of conventional, non-nanoform chemicals, funded by the German Federal Ministry for Education and Research, is currently under way (Lauenstein et al., 2012), their applicability for the testing of NMs has not yet been evaluated systematically.

PCLuS, typically cut to a thickness of approximately 200–300 μm, contain all the cell types present in the lung including those relevant for inducing immune responses, i.e. dendritic cells, macrophages, and mast cells (Henjakovic et al., 2008). Pulmonary morphology and organ-typical cell–cell structures enabling intercellular communication are maintained for up to 70 h (BéruBé et al., 2009; Martin et al., 1996). Thereby reflecting physiological pulmonary histology, the ex vivo PCLuS system has already been used to study a variety of scientific problems relating to the lung, ranging from pharmacological effects on the airway system (Martin et al., 1996), pulmonary function (Martin et al., 2000), and toxicological effects of bulk or nanoscale substances (Nassimi et al., 2009). Results from PCLuS studies have been evaluated to be precise and reproducible (Martin et al., 1996). However, also the contrary has been reported: BéruBé et al. (2009) warned against possibly large variations in the results obtained with replicate slices and with slices from different donors.

The test substances applied were the 16 NMs available at the onset of the present study in the repository of representative nanomaterials that the European Commission's Joint Research Centre (JRC) has established in support of the OECD WPMN's Sponsorship Programme (Singh et al., 2011; see also: http://ihcp.jrc.ec.europa.eu/our_activities/nanotechnology/nanomaterials-repository/list_materials_JRC_rep_oct_2011.pdf/view. Note: All websites were accessed in November 2013.) The NMs comprised anatase, rutile, and rutile-anatase titanium dioxide (TiO$_2$) nanomaterials, uncoated and coated zinc oxide (ZnO), silicon dioxide (SiO$_2$) and cerium (IV) oxide (CeO$_2$) NMs, monodispersed silver (Ag), and multi-walled carbon nanotubes (MWCNTs) of different lengths and diameters. This broad spectrum of NMs was selected with the aim of gaining an overview on the applicability of the PCLuS test method in determining the different types of effects elicited by different chemical types of NMs.

So far only a limited number of possible mechanisms of action have been discerned for NMs: direct interactions with cellular structures (such as membrane lysis), the catalyzing formation of reactive oxygen species (ROS), and inflammation (Landsiedel et al., 2010; Nel et al., 2009, 2013a,b; Shvedova et al., 2012). Metal oxide and metal NMs can exert cytotoxicity by dissolution and shedding of toxic ions, and carbon nanotubes can elicit pro-fibrogenic responses (Nel et al., 2013a).

The oxidative stress paradigm has been recognized to play a central role in the evolvement of NM toxic effects. Depending on their physico-chemical characteristics, NM-induced ROS can affect different intracellular structures and activate different enzymatic pathways, resulting in different types of cellular damage (Shvedova et al., 2012). In neutrophils, NM-induced ROS can activate myeloperoxidase, which has been reported to play an important role in the biodegradation of carbon nanotubes (CNTs; Kotchey et al., 2013; Shvedova et al., 2012). Activation of redox-sensitive signaling pathways by free radicals can lead to the induction of inflammatory mediators (Duffin et al., 2007a; Meng et al., 2009; Shvedova et al., 2012; Xia et al., 2008), whereas the selective activation of mitochondrial cardiolipin can lead to cellular apoptosis (Hussain et al., 2010; Shvedova et al., 2012). If primary cellular effects progress, local or systemic organ toxicity and genotoxicity can occur (Landsiedel et al., 2010). In the lung, apoptosis is involved in the pathogenesis of a variety of disorders, such as asthma, emphysema, and acute respiratory distress syndrome (Ahamed et al., 2011; Hussain et al., 2010). Non-ROS-dependent interference with the mitotic spindle apparatus might also lead to aneuploidy and ultimately, potentially, to cancer (Shvedova et al., 2012).

Based upon these considerations, the following endpoints were selected to investigate whether the spectrum of cellular effects that have been recorded for the different types of NMs can be reflected in the PCLuS test system: Severe tissue destruction (measured by loss of PCLuS total protein mass), cytotoxicity (WST-1-measured reduction in mitochondrial activity), apoptosis (caspase-3/-7 activation), oxidative stress (reduction or increase of intracellular GSH content), and inflammation, i.e. induction of interleukin-1α (IL-1α), tumor necrosis factor-α (TNF-α), cytokine-induced neutrophil chemoattractant-1 (CINC1; the structural and functional rat homologue to interleukin-8 (IL-8); Himi et al., 1997), monocyte chemoattractant protein-1 (MCP-1), macrophage-colony stimulating factor (M-CSF), and osteopontin (OPN).

These endpoints comply with the scientific advice (Hankin et al., 2011) on fulfilling information requirements for nanomaterials under the EU REACH regulation (Registration, Evaluation, Authorisation of Chemicals; Anon, 2006). Hankin and co-authors list cellular uptake, cell viability, oxidative stress, and inflammation amongst the relevant specific toxicological properties to be addressed as additional endpoints for NM risk assessment. Finally, histopathological evaluations of the PCLuS were performed to compare NM effects on in vitro cellular morphology to known histopathological effects upon in vivo NM exposure. Since PCLuS maintain the pulmonary tissue structure, histopathological evaluations provide an added value of this test system over cell culture test systems which only allow recording histological effects on the cellular, but not organ tissue level. Thus PCLuS histopathology might have the potential to link effects observed ex vivo to the in vivo situation.

Depending upon their size, inhaled nanomaterials (and their aggregates and agglomerates) can be deposited in the nasopharyngeal, tracheobronchial or alveolar regions of the respiratory tract. Approximately half of the dose of 20 nm nanomaterials will be deposited in the alveolar region (ICRP, 1994; Oberdörster et al., 1994). However, NMs can change their physico-chemical properties once dispersed in test substance vehicles (e.g. cell culture media) or upon reaching target cells (Landsiedel et al., 2010). They can undergo significant agglomeration or form a characteristic 'corona' by interacting with proteins and phospholipids present in the biological fluids (Feltis et al., 2012; Monopoli et al., 2011, 2012; Murdock et al., 2008; Schaefer et al., 2012). Since all of these changes can alter NM reactivity in biological systems, a defined dispersion protocol is an important part of any testing method for nanomaterials to ensure interpretability of test results. In the

present study a dispersion protocol was applied including sonication of the stock solution and addition of bovine serum albumin (BSA) to the cell culture medium to stabilize the dispersion.

Material and methods

Test substances and primary particle characterization

The 16 nanomaterials comprised six different titanium dioxide (TiO_2) nanomaterials (three anatase; NM-100, NM-101, NM-102; two rutile: NM-103, NM-104; and one rutile-anatase: NM-105), uncoated (NM-110) and coated (NM-111) zinc oxide, silicon dioxide (SiO_2) nanomaterials produced by precipitation (NM-200) and by thermal process (NM-203), uncoated cerium (IV) oxide (CeO_2) produced by precipitation (NM-211, NM-212), monodispersed silver (Ag) produced by precipitation (NM-300K), and 3 multi-walled carbon nanotubes (MWCNT) of different lengths and diameters (NM-400, NM-401, NM-402).

Information on the 16 NMs is provided in Table 1 listing the substance names, their OECD reference number, form of production, and form of delivery (powder or suspension). Table 1 further presents the nanomaterials' physico-chemical characteristics as provided by the JRC (Ispra, Italy), the supplier of all NMs.

All NMs were delivered as dry matter, except for Ag NM-300K, which was provided in dispersion. The Ag NM-300K dispersant is an aqueous solution containing the capping agents polyoxyethylene glycerol trioleate and polyoxy ethylene (20) sorbitan mono-laurat (Tween 20). This dispersant, on its own, was included as a further, 17th (non-nanoform) test substance (NM-300K DIS) to verify whether adverse effects induced by the Ag NM-300K dispersion were indeed caused by the nanoform silver, and not by its dispersant.

Preparation of test substance stock dispersions

Stock dispersions of the test substances were prepared taking into account personal recommendations from Z. Magdolenova (Health Effects Laboratory, Kjeller, Norway). As a rule, 3 mg of the test substances was added to 1 mL of the cell culture medium (serum-free Dulbecco's modified Eagle's medium with nutrition mixture F-12 HAM (DMEM/F-12; Invitrogen, Germany, Product No. 11039-047) containing 1% (v/v) Penicillin/Streptomycin (10 000 IU/10 000 μg/mL; Biochrom AG, Germany). Based upon the results of pre-tests determining the size distribution of the nanoparticles in solution, stock solution concentrations of 4, and 10, 15 mg/mL were selected for TiO_2 NM-103, ZnO NM-111, and TiO_2 NM-102, respectively, to ensure a sufficient amount of the test substance being dispersed in the final preparations. In the case of Ag NM-300K, the stock dispersion concentration of 1 mg/mL was chosen to take into account that this material was already fully dispersed in the solution provided by the supplier.

To homogenize the stock dispersion, it was shaken manually and then sonicated, cooled on ice: First, the samples were sonicated twice for 2.5 min with a probe sonicator at 200 Watt (Sonoplus Ultraschall-Homogenisator, Bandelin Electronic, Germany; power: 20-30%; cycle: 100%). Next the dispersion was vortexed for 10 s to disperse particles that might have attached to the inner wall of the flask (vortex: VWR international, USA). Afterwards, one part of a 5% BSA solution (w/v; i.e. 0.1 mL; Sigma-Aldrich, Germany) was added to nine parts stock dispersion, and one sonication step was repeated. Subsequently, the dispersion was stirred on a magnetic stirrer (IKA Labortechnik, Germany) at 700 rpm at room temperature for 24 h.

Characterization of the nanoparticles as prepared test items

Characterization of the NMs as prepared test items was performed using analytical ultracentrifugation (AUC) as described by Wohlleben (2012). Test substance stock dispersions were prepared 24 h before

application onto the PCLuS and were analyzed on the day of exposure using the Beckman Ultracentrifuge XLI™ with integrated interference optics (Beckman Coulter, Palo Alto, CA, USA). Based upon the AUC measurements, the amount and diameters of each fraction were calculated independently as described by Wohlleben (2012). Particle sedimentation fractions with particle diameters below 10 μm were recorded as 'dispersed concentration'. The results of this characterization are presented in Table 2a revealing that, apart from Ag NM-300K, SiO_2 NM-203, and the MWCNTs, all NMs underwent some degree of agglomeration, and all NMs adsorbed BSA.

Preparation of test substance solutions

The final dispersions were prepared out of the stock dispersions by adding cell culture medium. Based upon the respective dispersed concentrations of each of the NMs determined by AUC, the dilution factors were adapted to achieve final dispersed test substance concentrations of 10, 50, 100, 500, and 1000 μg/mL for all 16 NMs, corresponding to 0.3–300 μg/cm^2 surface area of the cell culture wells.

For dispersed Ag NM-300K, the dilution factors took into account that this nanomaterial was delivered in a 10.16% (w/w) dispersed form. For TiO_2 NM-100, the highest concentration was set at 840 μg/mL, the calculated dispersed concentration. For all other NMs, the dispersed concentration exceeded 1000 μg/mL so that this concentration could be set as highest test concentration. Test substance dispersions were prepared in glass vials with at least 5 mL cell culture medium in each vial. Before usage, the dispersions were stirred for at least 1 h at 700 rpm at room temperature.

Calculation of effective dose

AUC measurements were also used to determine the effective NM dose reaching the cells of the PCLuS taking into account the specific diffusion and gravitational settling properties of NMs (Hinderliter et al., 2010; see Supplementary Information (SI) for details on the calculation of the effective dose).

For agglomerated NMs, sedimentation is expected to be the predominant parameter determining the effective test substance dose reaching the PCLuS, and sedimentation was monitored directly by AUC. For well-dispersed NMs, however, diffusion properties have been recognized to determine the amount of particles reaching the tissue cultures and thus have to be included in effective dose calculations (Teeguarden et al., 2007). Such properties are not reflected by AUC. Therefore, for those NMs for which effective dosages of less than 50% of the test substance concentration was calculated via AUC (i.e. for which sedimentation obviously was not the predominant parameter), the effective dose was additionally calculated using the 'In Vitro Sedimentation, Diffusion, and Dosimetry' (ISDD) model (Hinderliter et al., 2010), which takes into account both NM sedimentation and diffusion properties (see also SI for further details on the ISDD model).

Preparation of precision cut lung slices (PCLuS)

The PCLuS were prepared from nulliparous and non-pregnant female Wistar Crl:WI (Han) rats (8 to 10 weeks old and free from clinical signs, obtained from Charles River Laboratories, Germany). All animal work was performed in an animal facility that holds a certificate from the International Association for Assessment and Accreditation of Laboratory Animal Care (AAALAC). The animal work was performed in accordance with the local regulatory agencies, and all study protocols were in compliance with the federal guidelines.

Animals were euthanized with an intraperitoneal overdose of pentobarbital sodium (concentration: 160 mg/mL, dose: 300 mg/kg body weight). The lung lobes and tissues and the lung slices were prepared as described previously (Wohlleben et al., 2011) using a

Table 1
Test substances and primary particle characterization provided by the supplier (European Commission's Joint Research Centre, Ispra, Italy).

OECD reference number	Test material	Mineral form, form of production, surface chemistry, physical state, catalytic activity and conductivity	Purity (%), impurities	Primary crystal size (Scherrer, nm), particle shape	Primary and mean particle sizes, specific surface area
NM-100	Titanium dioxide pigment	Anatase, uncoated, comparably large particle size within TiO2-NM-series	>98.5	XRD pending	PPS, TEM: 42–90 nm; MPS, TEM: 299 nm, 267 nm; SSA: 10 m²/g
NM-101	Titanium dioxide	Anatase, uncoated, high photocatalytical activity	91.7	8, XRD: 6	SSA: 320 m²/g
NM-102	Titanium dioxide	Anatase, uncoated, high photocatalytical activity	96.0	22, XRD: 20	SSA: 90 m²/g
NM-103	Titanium dioxide	Rutile, ultrafine, hydrophobic	89.0; Al₂O₃: 6.2%	20, XRD: 20	SSA: 60 m²/g
NM-104	Titanium dioxide	Rutile, ultrafine, hydrophilic	89.8; Al₂O₃: 6.2%	20, XRD: 20	SSA: 60 m²/g
NM-105	Titanium dioxide	Rutile-anatase, uncoated	>99	21, XRD: 22	SSA: 61 m²/g
NM-110	Zinc oxide	Uncoated, white powder	>99	70–200 (Horiba light scattering), spherical	PPS, XRD: 41.5 nm, SSA: 13 m²/g
NM-111	Zinc oxide	Coated with 1–4% triethoxycaprylyl silane, white powder	>99; coated modification: 96–99	XRD: 33.8, spherical	particle size < 200 nm; mean 130 nm, range 90–190 (Horiba light), SSA: 16 m²/g
NM-200	Synthetic amorphous silica PR-A-02	Silicon dioxide produced by precipitation, white powder	96.5	TEM: 20, spherical	primary particles in the 10–25 nm range, particles aggregated, SSA: 230 m²/g
NM-203	Synthetic amorphous silica PY-A-04	Silicon dioxide produced by thermal process, white powder	–	TEM: 20, spherical, irregular	primary particles in the 5–30 nm range, particles aggregated, SSA: 226 m²/g
NM-211	Cerium (IV) oxide	Cerium dioxide, uncoated, produced by precipitation, yellowish powder	>95	10.3, cubic	XPS: Ce:O ratio 1:2, SSA: 66 m²/g
NM-212	Cerium (IV) oxide	Uncoated, produced by precipitation, yellowish powder	>99.5	33, cubic	XPS: Ce:O ratio 1:2, SSA 28 m²/g
NM-300K	Silver < 20 nm	Produced by chemical precipitation of silver nitrate, monodispersed with capping agent (monolayer) stabilizing agents: 4% each of polyoxyethylene glycerol trioleate and polyoxy ethylene (20) sorbitan mono-laurat (Tween 20), silver content: 10.16% w/w, very viscous, concentrate orange-brown, yellow in dilution	10	colloidal, spherical	particle size, TEM: 15 nm, UVvis spectra: D90 < 20 nm (90% < 20 nm)
NM-300K DIS	Ag-dispersant (control material for NM-300K)	Aqueous solution containing the capping agents: 4% each of polyoxyethylene glycerol trioleate and polyoxy ethylene (20) sorbitan mono-laurat (Tween 20), very viscous	–	–	–
NM-400	Multi-walled carbon nanotubes	Specialty graphite, produced by CCVD, at 20 °C and 1013 hPa: solid powder, black odorless, insoluble in water or organic solvent, surface charge: NA, conductive	>90; impurities: <10% metal oxide	Ø 9.5, 1.5 µm length, short, thin, tangled, concentric tubes, presence of amorphous carbon on surface of tubes	SSA: 280 m²/g
NM-401	Multi-walled carbon nanotubes	Specialty graphite, produced by CCVD, at 20 °C and 1013 hPa: solid powder, black odorless, insoluble in water or organic solvent, surface charge: NA, conductive	>95, impurities: metal oxide < 5%	Ø 10–30, 5–15 µm length, short, thin, tangled, concentric tubes, presence of amorphous carbon on surface of tubes	SSA: 300 m²/g
NM-402	Multi-walled carbon nanotubes,	Specialty graphite, produced by CCVD, at 20 °C and 1013 hPa: solid powder, black odorless, insoluble in water or organic solvent, surface charge: NA, conductive	>90, metal oxide < 10%	Ø 5–15, 0.1–10 µm length, short, thin, tangled concentric tubes, presence of amorphous carbon on surface of tubes	SSA: 250–300 m²/g

- PPS: primary particle size; MPS: mean particle size; determined by transmission electron microscopy (TEM) or x-ray photoelectron spectroscopy (XPS).
- Primary crystal size; determined with x-ray diffraction (XRD), TEM, or dynamic light scattering (DLS)
- SSA: specific surface area; determined by the method of Brunauer–Emmett–Teller)
- CCVD: catalytic chemical vapor deposition

Krumdieck tissue slicer (Alabama Research and Development, USA) to obtain precision-cut lung slices with a diameter of 8 mm and a thickness of approximately 200–250 µm.

To ensure reproducible quality of the PCLuS, only rats of the age of 8 to 10 weeks were used, which is the same age of rats in in vivo inhalation studies. Thereby all organs used for PCLuS cutting were of comparable size, so that constant amounts of PCLuS (90–120 slices per animal) were obtained. During lung preparation, care was taken that the temperature of the agarose-medium solution used to fill the lungs prior to slice cutting did not exceed body temperature and that the amount of solution applied did not increase organ pressure, thereby avoiding physical destruction of the lung tissues. For the core cut, the crucial step in the

Table 2a

Characterization of the particles dispersed in bovine serum albumin (BSA)-containing cell culture medium determined by AUC: Mean particle diameter, weight percentage of dispersed particles (<10 μm), and concentration of non-adsorbed BSA.

OECD reference number	Test material	NM diameter with BSA (nm)	Dispersed NM (weight%)	Non-adsorbed BSA (mg/mL)
NM-100	TiO_2	262	28	2.4
NM-101	TiO_2	428	39	2.5
NM-102	TiO_2	495	22	3.2
NM-103	TiO_2	118	22	2.6
NM-104	TiO_2	105	48	3.1
NM-105	TiO_2	79	66	2.8
NM-110	ZnO	176	75	2.2
NM-111	ZnO	310	33	2.6
NM-200	SiO_2	65	47	2.8
NM-203	SiO_2	58	125	2.9
NM-211	CeO_2	146 and >309[a]	43	3.0
NM-212	CeO_2	107	84	3.2
NM-300K	Ag	11	100	3.6
NM-400	MWCNT	30	90	2.7
NM-401	MWCNT	219	94	3.5
NM-402	MWCNT	36	96	2.8

- AUC: analytical ultracentrifugation
- [a] Bimodal mean particle size distribution

preparation, only very sharp knives were used to minimize cellular damage. Transfer of the prepared PCLuS to the vials or cell culture wells was performed with a round device only, taking care not to squeeze the tissues.

PCLuS exposure to test substances, negative and positive controls

For exposure of the PCLuS to the test substance, two lung slices per well were transferred to a 24-well plate and incubated in 500 μL cell culture medium for 24 h under cell culture conditions (37 °C, 5% CO₂, 95% humidity). Applying two slices of a thickness of approximately 250 μm each per well (and not e.g. one slice twice the thickness) ensured that sufficient tissue material was exposed to the test substances and that all cells of the slices could come into contact with the cell culture medium and the test substances.

Additional two slices per well were used for incubations of the negative and positive controls. DMEM/F-12 medium was used as negative control (NC). The following positive controls (PC) were used, dissolved in 500 μL solution, to verify test system inducibility:

- 0.1% Triton X-100 (Sigma Aldrich, Germany) for the cytotoxicity assay and for histopathology;
- 0.5 μM staurosporine (Sigma Aldrich, Germany) for the caspase-3/-7 assay;
- 10 mM DL-buthionine-[S,R]-sulfoximine (BSO) (Sigma Aldrich, Germany) for the GSH assay.

For the cytokine release assays, the suitability of 100 ng/mL lipopolysaccharide (LPS) (Sigma Aldrich, Germany) as PC was investigated. LPS is commonly used as PC in cytokine assays (Feltis et al., 2012; Henjakovic et al., 2008; Switalla et al., 2010a). However, LPS has a different mode of immunological action than NMs: Being bacterial products, LPS bind to toll-like receptors 2 and 4 that modulate pathogen-induced immune reactions (Janardhan et al., 2006; Lorne et al., 2010; Saito et al., 2005). NMs, on the other hand, are engineered particles causing generalized neutrophilic or eosinophilic inflammatory responses (Cho et al., 2010; Feltis et al., 2012). Specifically, in rats LPS has been observed to induce IL-1α, TNF-α, CINC1 (IL-8), and in some cases, M-CSF, but not OPN or MCP-1 (unpublished in-house data). Thus LPS does not induce all of the tested cytokines. Furthermore LPS measurements frequently had high coefficients of variation and repeatedly did not meet the respective PC-related acceptance criteria (see below). Therefore it was decided not to use LPS as PC in the cytokine assays, and calculation of the x-fold increase of test substance results in relation to the NC was applied instead to verify test system inducibility in the cytokine assays.

Assay performance

After incubating the PCLuS with the respective test substance and control solutions for 24 h,

- Reduction in mitochondrial activity (WST-1 assay) was measured directly in the PCLuS, just as histopathology was performed using intact PCLuS.
- Intact PCLuS were also submitted to the caspase-3/-7 activation assay, where PCLuS lysation however was the first step of the commercial test kit (see below).
- Total protein content, glutathione content, and intracellular interleukin-1α (IL-1α) were determined in lysates of exposed PCLuS, and
- PCLuS supernatants were used to determine the levels of the extracellular cytokines (see below).

For preparation of the PCLuS lysates for GSH and IL-1α measurements, the two PCLuS of each well were freeze–thawed three times in 1 mL phosphate-buffered saline (PBS buffer; Biochrome AG, Germany) containing 2 mM EDTA (Biochrome AG, Germany) and 0.2% protease inhibitor cocktail (Sigma Aldrich, Germany). During this procedure, tissues were shock-frozen in liquid nitrogen and then thawed in a water bath at 37 °C three times each. Thereby the cell–cell interactions are destroyed. After centrifugation (20 min at 6000 g; centrifuge Rotina 35R/Hettich AG, Switzerland), intracellular glutathione and IL-1α are present in the PBS buffer. This supernatant was collected and stored at −80 °C until glutathione and IL-1α were determined.

All tests were performed in duplicate (biological replicates), and all measurements were performed twice (technical replicates). Test results are expressed as means of the technical and biological replicates further indicating the distance of the lower and upper technical means to the overall mean value.

Determination of protein content of PCLuS. The colorimetric BCA (bicinchoninic acid) protein assay (Pierce® BCA Protein Assay Kit; Thermo Fisher Scientific, Inc., USA) was performed to determine the protein content of the PCLuS. This assay combines the reduction of Cu^{2+} to Cu^{1+} by protein in an alkaline medium with the colorimetric detection of Cu^{1+} cations by BCA (http://www.piercenet.com/browse.cfm?fldID=02020101).

To prepare PCLuS lysates for the protein content measurements, the two lung slices present in each well were transferred to lysis buffer (500 μL of 0.1% Triton X-100 in PBS) containing 0.2% (v/v) protease inhibitor cocktail (Sigma Aldrich, Germany) and incubated under cell culture conditions for 1 h. Cell lysates were centrifuged for 3 min at

1000 g and 4 °C and supernatants stored at −80 °C until determination of protein content.

For determination of the total protein content, 200 μL BCA working reagent were added to 25 μL of the PLuCS lysates in a clear 96-well plate and mixed carefully. The plate was incubated under cell culture conditions for 30 min. Total protein content was measured as net absorbance at 570 nm in a multilabel counter (Wallac Victor 3 1420, Perkin Elmer, USA) using BSA as a standard. For each test run, sigmoidal BSA standard curves were prepared and calculated using the GraphPad Prism6® software in a free trial version for Mac (www.graphpad.com).

The determination of PCLuS protein mass served several purposes:

- First, it was used as a quality control to verify acceptable thickness of the lung slices, as reflected by total protein contents between 150 and 450 μg/mL (based upon unpublished historical data from BASF). All PCLuS (used in non-cytotoxic measurements) met this premise.
- Second, it was used to recognize NMs causing severe tissue destruction, as reflected by reductions in total protein below 150 μg/mL, i.e. below the lowest NC measurement.
- Third, it was used to relate the cytotoxicity test results to tissue mass of the PCLuS. (Since the lung slices had to be lysated for conducting the BCA protein assay, only cytotoxicity test results could be related to PCLuS total protein since only the WST-1 assay does not require lysating the tissue slices).

Of note, the determined total protein content most likely to also includes a proportion of the bovine serum albumin that had been added to the NM dispersions, as was evident, e.g. from the histopathological evaluations where nanoparticles were present in the tissue slices. However, this proportion of BSA was considered to be negligible since only one part of the 5% BSA solution had been added to nine parts of the stock solution during preparation of the NM stock solutions, and no further BSA had been added during preparation of the final test substance concentrations.

Determination of cytotoxicity (i.e. changes in mitochondrial activity). Cytotoxic effects of the NMs were assessed by measuring changes in mitochondrial activity (determined via reduction of water-soluble tetrazolium WST-1 to formazan using the Cell Proliferation Reagent WST-1; Roche, Germany). PCLuS were incubated for 2 h under cell culture conditions with 500 μL WST-1 reagent (1:10 final dilution in culture medium) per well. Prior to testing, the test substance supernatants were centrifuged for 5 min at 300 g to collect the nanoparticles at the bottom of the wells. Afterwards 100 μL supernatant were transferred to a clear 96-well plate and measured in a multilabel counter (Wallac Victor 3 1420, Perkin Elmer, USA). Formazan absorbance (optical density, OD) was measured at 450 nm with a reference wavelength of 690 nm. The absorbance values were expressed in relation to the total protein (TP) content of the respective lung slices (OD/TP).

Determination of caspase-3/-7 activation. Caspase-3 and -7, two cysteine aspartic acid-specific proteases, have been recognized to coordinate the execution phase of apoptosis by cleaving multiple structural and repair proteins thereby playing key effector roles in apoptosis (Hussain et al., 2010; Slee et al., 2001). Therefore, apoptotic reactions of the NMs were evaluated by determining activation of caspase-3 and -7, using the Caspase-Glo® 3/7 Assay (Promega Corporation, USA), which was performed directly using the two PCLuS of each well.

The tissue slices intended for measurement of caspase-3 and -7 activities were transferred to 300 μL Caspase-Glo® 3/7 Reagent per well of a 24-well plate. This reagent induces cell lysis, followed by caspase cleavage of the substrate, and generation of the luminescent signal. Upon addition of the reagent, the slices were incubated for 60 min at room temperature in the dark. Afterwards 100 μL supernatants were transferred to a luminescence-capable, black 96-well plate. (Due to the fibrous shape of the MWCNT, the respective supernatants were centrifuged at 100 000 g for 30 min before testing to prevent

test substance interference with the luminescence reaction.) Luminescence (expressed in Relative Luminescence Units; RLU) was read in a multilabel counter (Wallac Victor 3 1420, Perkin Elmer, USA). PCLuS treated with staurosporine were used as positive control. Positive control measurements were set as 100% caspase-3/-7 induction, and test results were expressed relative to the positive control.

Determination of oxidative stress. Glutathione (GSH) is an important intracellular antioxidant defending cells against harmful compounds (Monteiller et al., 2007; Pastore et al., 2003). Therefore oxidative stress was determined by measuring changes in cellular glutathione using the GSH-Glo™ Glutathione Assay (Promega Corporation, USA). This luminescence-based assay is performed in two steps, i.e. the GSH reaction and the luciferin detection. For the first step, 50 μL of tissue extract and 50 μL GSH-Glo™ Reagent 2× were added to a luminescence capable, black 96-well plate and incubated for 30 min at room temperature in the dark. Thereafter 100 μL reconstituted Luciferin Detection Reagent were added to each well, mixed briefly on a plate shaker (ZLE 164, Amersham, United Kingdom), and incubated again under the same conditions. (Due to the fibrous shape of the MWCNT, the respective supernatants were centrifuged at 100 000 g for 30 min before testing to prevent test substance interference with the luminescence reaction.) After 15 min, the resulting luminescence (expressed in RLU) was read in a multilabel counter (Wallac Victor 3 1420, Perkin Elmer, USA). PCLuS treated with BSO were used as positive control. The luminescence measured in the negative control (untreated PCLuS) was set as 100% amount of GSH, and test results were expressed relative to the negative control.

Determination of cytokine induction. Pre-tests were performed with TiO₂ NM-105, ZnO NM-110, and MWCNT NM-400 to determine which cytokines were best induced in PCLuS. For this purpose, samples of PCLuS supernatants and extracts frozen at −80 °C were sent to Myriad RBM (Myriad Rules-Based Medicine, Austin, TX, USA). Using xMAP technology (Luminex Corporation, Austin, TX, USA), 56 different cytokines from either the supernatant or PCLuS extract were measured. Based upon the results of these pre-tests and taking into account cytokine measurements in bronchoalveolar lavage and lung tissue homogenate from in vivo inhalation studies, induction and secretion of the following inflammatory mediators were determined:

Measured intracellularly, IL-1α, and measured extracellularly in the PCLuS supernatant, TNF-α, CINC-1 (IL-8), MCP-1, M-CSF, and OPN. These cytokines reflect three different stages and aspects of inflammation as recommended by Ma-Hock et al. (2009a): Mediators modulating immune reactions (IL-1α and TNF-α); mediators inducing infiltration of inflammatory cells into the lung tissue (CXC-chemokines, e.g. CINC1 (IL-8); and CC-chemokines, e.g. MCP-1); mediators inducing proliferation of hematopoietic cells (M-CSF) or sessile cells present in the lung (OPN).

The external pre-test cytokine measurements were repeated in-house for MWCNT NM-400. For technical reasons, they could not be repeated for TiO₂ NM-105. For completeness, the RBM-gained cytokine induction data for this NM are presented in the respective tables (Supplementary Information (SI) Tables S6-S10), however were excluded from the evaluation due to methodological differences.

The following commercial assays were used:

- DuoSet rat IL-1α/IL-1 F1; cat. no. DY500; R&D Systems, Inc., USA;
- Flow Cytomix Simplex Kit TNF-α, cat. no. BMS 8622 FF, eBioscience, Vienna, Austria;
- Quantikine rat CINC1, cat. no. RCN100, R&D Systems, Inc., USA;
- Flow Cytomix Simplex Kit MCP-1 rat, cat. no. BMS 8631 FF, eBioscience, Vienna Austria;
- Quantikine Mouse M-CSF, cat no. MMC00, R&D Systems Inc., USA;
- Quantikine mouse osteopontin, cat. no. MOST00; R&D Systems, Inc., USA.

The cytokine assays were performed with three test substance concentrations, i.e. 10, 100, and 1000 μg/mL. For MWCNT NM-400, the highest test substance concentration was 500 μg/mL. The Flow Cytomix assays (Fluorescence Bead Immunoassay; FBIA) were applied on a FACSCalibur™ flow cytometer (Becton Dickinson, Germany) using the FlowCytomix Pro Software (version 2.3, Bender MedSystems, Austria) for evaluations. The DuoSet and Quantikine ELISAs were performed with a Sunrise™ MTP Reader (Tecan AG, Switzerland) using the Magellan Software provided by the instrument producer. All assays were validated with the PCLuS extract or culture supernatant (see assay criteria in the Supplementary Information, Table S1). Test results were expressed as x-fold increase of cytokine levels relative to the negative control.

Histopathology. For histopathological investigations, the PCLuS were fixed immediately after exposure for a minimum of 24 h in approximately 1 mL 4% formaldehyde solution (BASF SE, Germany) followed by the preparation of Hematoxylin and Eosin (Sigma, Germany) stained cross sections. Triton X-100-treated PCLuS were used as positive controls for histopathological evaluation. Histopathological evaluations were not performed for PCLuS tested on TiO$_2$ NM-105, ZnO NM-110, or MWCNT NM-400.

Statistical analysis

Test substance availability and stability only allowed one run of tests for each of the nanomaterials. To assess the reliability of test results and test runs, specific test result-, NC- and PC-related acceptance criteria (AC) were laid down for all assays (Lauenstein et al., 2012). As regards test result-related AC, for the protein and WST-1 assays, the maximum difference between 2 technical replicates was set to be ≤0.3 OD; and for the GSH and caspase-3/-7 assays, the maximum difference between duplicate RLU measurements relative to the mean value of duplicate RLU measurements was set to be ≤30%. All test results of all assays fulfilled these test result-related AC.

The NC-related AC served to determine the intactness and viability of the tissue slices and the PC-related AC to determine PCLuS inducibility by a known reacting substance. The threshold values for these AC were set based upon the respective values laid down by Lauenstein and co-authors taking into account the overall results of the study at hand. An overview of the respective NC- and PC-related AC laid down for each assay is provided in Table 9).

Test results were excluded from further evaluation if the NC-related or PC-related AC were not met. By derogation of this provision, test results were included on a case-by-case basis, if statistical significance of the test results indicated that test results were sufficiently different from high negative control values (in the case of failure of the NC to meet NC-related AC) or that the test system had been inducible in spite of the failure of the PC to meet the PC-related AC. To determine statistical significance of test results (p ≤ 0.05), linear dose-responses were evaluated by testing for linear trend (95% significance level) using the EXCEL function RGP.

Additionally, NC confidence intervals, i.e. 95% prediction limits of the NC, were calculated with EXCEL from the means of all NC of a given assay and their standard deviation (STD) according to the formula [mean +/− (root(1 + 1/N)*t(N-1) *STD], with [t(n-1)] being the fractil of the t distribution with n-1 degrees of freedom. Thereby threshold values were determined above which measurements were considered to be biologically relevant, i.e. exceeding the range of values recorded for the NC. If no statistically relevant test results were recorded in test runs in which the NC exceeded the 95% confidence limit of the mean of all NC, it could not be determined whether this lack of effect was an artifact due to high NC reactivity or if it was indeed an indication of a lack of biological effect.

To determine intra-laboratory assay reproducibilities, coefficients of variation (CV%) exceeding 20% or 50%, respectively, were recorded.

These CV% threshold values were set in accordance to intra-assay and inter-assay precision values provided by test kit suppliers or reported in the literature (see Table 9) adjusted to comply with assay variabilities observed in previous PCLuS studies (Lauenstein et al., 2012; Wohlleben et al., 2011).

Results

Calculation of effective dose

The results of the AUC and ISDD calculations of the effective NM dosages reaching the PCLuS after 12- and 24-hour test substance exposure are presented in Table 2b. Making use of the AUC measurements of sedimentation, vast differences in the relative effective dosages ranging from 100% and 99% (for TiO$_2$ NM-100 and ZnO NM-110, respectively, corresponding to 300 and 297 μg/cm^2 for the highest test substance concentration of 1000 μg/mL) down to 2% for MWCNT NM-400 and NM-402, each, were recorded (corresponding to 6 μg/mL for the 1000 μg/mL test substance concentration). Also within the group of TiO$_2$ NMs, differences in the relative effective dosages between 100% (NM-100) and 44% (NM-105) were calculated by AUC sedimentation estimations. The differences in relative effective dosages observed for the SiO$_2$ NMs (81% for NM-200 versus 24% for NM-203), are likely to be explained by differing agglomeration stabilities of these two materials, since both SiO$_2$ NMs have similar primary and secondary characteristics (Tables 1 and 2a).

Based upon the ISDD calculations, effective dosages of the 1000 μg/mL (300 μg/cm^2) test substance concentration were calculated ranging from 80 μg/cm^2 for ZnO NM-111 down to 17 μg/cm^2 for MWCNT NM-401 (after 24 h test exposure). As compared to the AUC calculations, the ISDD effective dosage values were lower for the moderately dispersed TiO$_2$ NM-105, ZnO NM-111, and SiO$_2$ NM-200, but higher for the 'fully' dispersed particles (below 10% effective dose in AUC), i.e. SiO$_2$ NM-203, Ag NM-300K, and all MWCNT.

Considering that diffusion properties were not taken into account for the AUC-based calculations and that the critical parameter of number of particles in the individual agglomerates was chosen rather arbitrarily for the ISDD calculations, both approaches only provide estimations of the effective dosages. The respective values obtained with either method, nevertheless are in comparable ranges (Table 2b).

In vitro–in vivo comparisons are based upon the assumption that the effective dose reaching 1 cm^2 of tissue culture in vitro corresponds to the effective dosage reaching 1 cm^2 of lung surface in vivo. Comparing the AUC and ISDD calculations (for the strongly agglomerated and well dispersed NMs, respectively) to highest in vivo dosages (as determined in previous rat short-term inhalation studies) reveals that the effective in vitro dosages of the highest test substance concentration of 1000 μg/mL were consistently higher than the respective in vivo dosages, i.e. by orders of magnitude of at least 100 (Table 2b). Hence, the lowest test substance concentration of 10 μg/mL is more likely to reflect dosages applied in vivo.

Since, however, the focus of the present study aimed at determining the applicability of the PCLuS test system in detecting the spectrum of early cellular effects that may be caused by NMs, the dose range of 10–1000 μg/mL was maintained throughout the study to ensure inducing observable effects in all of the endpoint-specific assays.

Fulfillment of acceptance criteria and test result reproducibility

An overview of the fulfillment of the respective assay-specific NC- and PC-related AC is presented in Table 9 (with details in SI Tables S2–S11). Accordingly, all NC and PC fulfilled the respective AC in the BCA protein assay, and in the WST-1 assay, only the NC for CeO$_2$ NM-212 did not meet the NC-related AC. Since however significant cytotoxicity was measured for this substance at 1000 μg/mL, it was included in the evaluation. The proportion of NC not meeting their respective AC was

Table 2b

Estimation of effective dose of the 1000 μg/mL test substance concentration of 16 OECD reference nanomaterials reaching the PCLuS after 12- and 24-hour test substance exposure as calculated via analytical ultracentrifugation (AUC) and via ISDD model for well-dispersed NM (defined as <50% effective 24 h-dose determined by AUC-based calculations).

OECD reference number	Test material	% Dose after 12 h (AUC)	% Dose after 24 h (AUC)	Corresponding to μg/cm² (a)	Dose (μg/cm²) after 12 h (ISDD)	Dose (μg/cm²) after 24 h (ISDD)	Highest in vivo dose in STIS (b)
NM-100	TiO₂	97	100	300	–	–	
NM-101	TiO₂	46	62	186	–	–	
NM-102	TiO₂	66	82	246	–	–	
NM-103	TiO₂	32	60	180	–	–	
NM-104	TiO₂	26	48	144	24	35	
NM-105 (c)	TiO₂	24	44	132	25	38	0.4 μg/cm² (50 mg/m³) 0.56 μg/cm² (88 mg/m³)
NM-110	ZnO	90	99	297	–	–	
NM-111	ZnO	84	96	288	80	80	0.17 μg/cm² (12.5 mg/m³)
NM-200 (c)	SiO₂	15	27	81	23	32	0.09 μg/cm² (25 mg/m³)
NM-203	SiO₂	4	8	24	23	32	
NM-211	CeO₂	64	87	261	–	–	0.07 μg/cm² (25 mg/m³)
NM-212	CeO₂	43	68	204	–	–	0.13 μg/cm² (25 mg/m³)
NM-300K (c)	Ag	2	4	12	53	69	
NM-400 (c)	MWCNT	1	2	6	33	46	0.01 μg/cm² (2.5 mg/m³)
NM-401 (c)	MWCNT	Not determined	Not determined		12	17	
NM-402 (c)	MWCNT	1	2	6	30	42	

AUC: calculation of effective dose based upon analytical ultracentrifugation (AUC) measurements;

ISDD: calculation of effective dose making use of the 'In Vitro Sedimentation, Diffusion, and Dosimetry' (ISDD) model (Hinderliter et al., 2010)

Not determined: determination not possible for technical reasons

(a) Corresponding tissue culture surface area-based concentrations upon 24 h test substance exposure as calculated for the highest test substance concentration (1000 μg/mL = 300 μg/cm²)

(b) STIS: Short-term inhalation study; dosages based upon Ma-Hock et al. (2009a) for TiO₂ NM-105; Klein et al. (2012) for NM-111 and a substance similar to SiO₂ NM-200; unpublished in-house data for CeO₂ NM-211 and NM-212; and Ma-Hock et al. (2009b) for MWCNT NM-400.

(c) ISDD calculations taking into account

- NM density as determined with a water pycnometer (densities: NM-105 = 4.2 g/cm³; NM-200 = 2.2 g/cm³; NM-300K = 10.49 g/cm³; NM-400 = 1.8 g/cm³; NM-401 = 1.8 g/cm³; NM-402 1.8 g/cm³). Of note, NM density did not influence on effective dose: Calculating effective MWCNT dose with density = 1.02 provided the same results indicating that for these substances, transport is dominated by diffusion and not by particle deposition.

- NM primary particle size (see Table 1)

- NM hydrodynamic diameter in test substance dispersions (see Table 2a)

highest in the GSH, IL-1α, and OPN assays. Some degree of tissue damage is most likely to have occurred during PCLuS preparation or handling in those NC that failed to meet the respective NC-related acceptance criteria. Failure to meet the PC-related AC was most pronounced in the caspase-3/-7 assay.

Test runs, in which the NC exceeded 95% of the confidence limit of the mean of all NC of the respective assay (and in which no statistically significant test results were recorded), occurred three times each in the GSH and MCP-1 assays, twice in the TNF-α assay, and once each in the caspase-3/-7 and CINC1 assays (SI Tables S4, S5, S7, S8, S9). As discussed above, in these test runs, it is not possible to determine whether the lack of statistically significant effect truly reflects a lack of biological activity.

Test result reproducibility also was best in the BCA protein and WST-1 assays (Table 9 with details in SI Tables S2–S11). In the protein assay, 7 of 119 (6%) test results had CV% >20%. In the WST-1 assay, 5 of 91 test results had CV% >20% and one additional test result a CV% >50% (together: 7%). In contrast, in the GSH and caspase-3/-7 assays, 23 and 13 of 81 test results (28% and 16%), respectively, had CV% >20%. In the cytokine assays, up to half of the test results had CV% >20%.

PCLuS tissue destruction

For the following test substances, the PCLuS test system resulted in protein concentrations below the threshold limit of 150 μg/mL, pointing to severe PCLuS tissue destruction: for ZnO NM-110 at all test substance concentrations (10–1000 μg/mL), for ZnO NM-111 at 10, 500, and 1000 μg/mL, for Ag NM-300K at 50–1000 μg/mL, and for Ag dispersant NM-300K DIS at 1000 μg/mL (Table 3 and SI Table S2). The latter results reveal that the silver nanomaterial is more toxic than its dispersant. Therefore the dispersing agent did not predominantly cause the effects observed for Ag NM-300K. Since tissue destruction is an overriding effect, further investigations were not performed with these four substances.

Cytotoxicity

For a total of six test substances, the PCLuS test system revealed significant cytotoxicity, as determined by reduced mitochondrial activity in the WST-1 assay: for TiO₂ NM-100 at 500 and 1000 μg/mL, for TiO₂ NM-101 at 100, 500, and 1000 μg/mL, for both CeO₂ NM-211

Table 3

OECD reference nanomaterials causing PCLuS tissue destruction.

NM; μg/mL	NM-110 ZnO	NM-111 ZnO	NM-300K Ag	NM-300K DIS Ag dispersant
NC	275.1 ± 19.2	422.0 ± 28.4	241.8 ± 29.2	196.5 ± 15.5
10	149.7 ± 8.0	145.0 ± 5.9	172.7 ± 5.3	190.7 ± 1.0
50	130.4 ± 12.3	162.1 ± 2.9	107.1 ± 8.3	206.0 ± 0.3
100	134.4 ± 11.4	161.3 ± 0.0	83.5 ± 28.6 [a]	195.1 ± 1.8
500	135.1 ± 3.5	144.0 ± 2.3	67.0 ± 1.3	193.8 ± 19.8
1000	126.4 ± 12.8	138.5 ± 23.9 [a]	50.1 ± 4.4	60.9 ± 1.9
PC	63.4 ± 7.4	65.3 ± 3.2	19.5 ± 4.1 [a]	19.4 ± 0.3

- Total protein content (μg/mL); all data expressed as mean of duplicate testing and distance of upper and lower value to mean
- PCLuS tissue destruction: PCLuS total protein content <150 μg/mL as determined in the Pierce® BCA protein assay
- a: CV% >20%

Table 4
OECD reference nanomaterials causing significant cytotoxicity in PCLuS in the WST-1 assay at concentrations not causing tissue destruction (cf. Table 3).

NM; μg/mL	NM-100 TiO$_2$	NM-101 TiO$_2$	NM-211 CeO$_2$	NM-212 CeO$_2$	NM-401 MWCNT	NM-402 MWCNT
NC	47.4 ± 5.7[a]	49.8 ± 2.2	66.4 ± 5.3	28.4 ± 1.1[c]	63.4 ± 0.1	69.1 ± 4.2
10	53.8 ± 2.9	50.2 ± 5.3	66.0 ± 0.1	33.6 ± 1.5	61.1 ± 3.5	58.7 ± 3.5
50	45.7 ± 3.1	45.4 ± 2.3	71.4 ± 3.9	34.0 ± 3.0	74.9 ± 1.8	63.0 ± 2.2
100	43.5 ± 5.8	42.6 ± 2.8*	73.4 ± 2.0	30.9 ± 0.7	66.1 ± 0.5	61.1 ± 0.3
500	38.8 ± 3.9*	41.1 ± 4.2*	60.3 ± 2.4	29.3 ± 0.3	61.8 ± 1.7	40.7 ± 0.0*
1000	41.0 ± 2.0*	38.8 ± 1.3*	61.0 ± 3.6*	27.3 ± 0.7*	49.0 ± 1.7*	43.5 ± 2.0*
PC	37.2 ± 20.8[b]	16.9 ± 0.8	10.8 ± 0.5	10.3 ± 0.5	13.7 ± 0.5	20.9 ± 1.2[a]

- NC: negative control (DMEM/F12); PC: positive control (Triton X-100)
- OD: optical density; TP: total protein
- All data expressed as mean OD of duplicate testing related to mean PCLuS protein contents of the respective well (TP) and distance of upper and lower value to mean
- The highest test substance concentration for NM-100 was 840 μg/mL, i.e. its calculated dispersed concentration
- a: CV% > 20%
- b: CV% > 50%
- c: NC did not meet respective acceptance criterion
- *Statistical significance (p ≤ 0.05) in trend analysis

Table 5
OECD reference nanomaterials causing significant changes in caspase-3/-7 activities in PCLuS.

NM; μg/mL	NM-100 TiO$_2$	NM-200 SiO$_2$
NC	34.9 ± 2.5	30.1 ± 5.0[a]
10	33.1 ± 0.7	37.2 ± 1.6
50	35.7 ± 3.8	36.1 ± 4.4
100	34.8 ± 1.3	33.6 ± 1.8
500	53.0 ± 0.2*	41.7 ± 4.2*
1000	46.8 ± 3.1*	39.7 ± 0.1*
PC	70 600 ± 7303 = 100.0%	87 744 ± 6494 = 100.0%

- NC: negative control (DMEM/F-12); PC: positive control (Staurosporine); RLU: Relative Luminescence Unit
- Caspase-3/-7 assay:
  RLU expressed relative to PC which was set as 100% and distance of upper and lower value to mean
- a: CV% > 20%
- *Statistical significance (p ≤ 0.05) in trend analysis

and NM-212 and for MWCNT NM-401 each at 1000 μg/mL, and, for MWCNT NM-402 at 500 and 1000 μg/mL (Table 4 and SI Table S3).

Caspase-3/-7 activation

Significant activation of caspase-3 and -7 without corresponding cytotoxicity in the PCLuS test system was induced by SiO$_2$ NM-200 at 500 and 1000 μg/mL. Significant activation of caspase-3 and -7 with concurrent significant cytotoxicity was recorded for TiO$_2$ NM-100 at test substance concentrations 500 and 840 μg/mL (Table 5 and SI Table S4).

Regardless of cytotoxicity, for TiO$_2$ NM-100 and SiO$_2$ NM-200 (significant caspase activation), as well as TiO$_2$ NM-101, NM-102, NM-103, and SiO$_2$ NM-203 (non-significant caspase activation), the highest RLU measurements were obtained at the second highest test substance concentration (500 μg/mL), and for TiO$_2$ NM-105 and MWCNT NM-400, at 100 μg/mL (non-significant caspase activation) (Table 5 and SI Table S4).

Oxidative stress

Due to overriding cytotoxicity, only test results obtained at non-cytotoxic test substance concentrations were evaluated in the GSH assay. In the PCLuS test system, significant changes in intracellular GSH content at non-cytotoxic test substance concentrations were elicited by TiO$_2$ NM-101 at 10 and 50 μg/mL, by TiO$_2$ NM-102 and NM-104 at 1000 μg/mL, and by MWCNT NM-401 at 500 μg/mL. In all cases, increases in GSH content were measured, presumably reflecting a cellular defense response to ROS. For no test substance significant reductions in GSH content were determined, (Table 6 and SI Table S5).

Cytokine induction

A total of 12 NMs were evaluated in the cytokine induction assays, i.e. all NMs that were not ruled out due to overriding tissue destruction additionally excluding the test results obtained for TiO$_2$ NM-105 in the external laboratory due to methodological differences (see above; Material and methods; Determination of cytokine induction), and once more excluding cytotoxic test substance concentrations from the evaluation.

Table 6
OECD reference nanomaterials causing significant changes in GSH levels in PCLuS at concentrations causing neither tissue destruction nor cytotoxicity, (cf. Tables 3 and 4).

NM; μg/mL	NM-101 TiO$_2$	NM-102 TiO$_2$	NM-104 TiO$_2$	NM-401 MWCNT
NC	14 376 ± 705 = 100.0%	11 649 ± 1216 = 100.0%	18 676 ± 2623 = 100.0%	6368 ± 284 = 100.0%[c]
10	133.5 ± 0.1*	122.5 ± 7.5	84.0 ± 11.0	82.5 ± 20.5[a]
50	149.6 ± 17.1*	112.5 ± 2.6	72.4 ± 11.3[a]	85.3 ± 6.8
100	Cytotoxicity	122.8 ± 3.8	81.4 ± 0.3	87.0 ± 3.9
500	Cytotoxicity	113.5 ± 0.7	85.8 ± 8.0	111.1 ± 0.8*
1000	Cytotoxicity	136.1 ± 3.8*	115.1 ± 15.7*	Cytotoxicity
PC	24.0 ± 0.2	27.9 [d]	16.7 [d]	27.9 ± 1.4

- NC: negative control (DMEM/F-12); PC: positive control (DL-Buthionine-[S,R]-sulfoximine); RLU: Relative Luminescence Unit
- GSH assay:
  RLU expressed relative to NC which was set as 100% and distance of upper and lower value to mean
- a: CV% > 20%
- b: CV% > 50%
- c: NC did not meet respective acceptance criterion; d: only one measurement
- *Statistical significance (p ≤ 0.05) in trend analysis

Table 7
OECD reference nanomaterials causing significant changes in cytokine induction (pg/mL) in PCLuS at concentrations causing neither tissue destruction nor cytotoxicity, (cf. Tables 3 and 4).
Note: Joint footnotes for Table 7a–f at bottom of Table 7f.

Table 7a - OECD reference NM causing significant IL-1α induction (x-fold of NC; NC: pg/mL) in PCLuS at non-cytotoxic concentrations

NM; μg/mL	NM-101 TiO$_2$	NM-104 TiO$_2$	NM-200 SiO$_2$
NC	200 = 1.0	500 = 1.0	400 = 1.0 [a]
10	1.8 *	1.0	1.1 [a]
100	cytotoxicity	1.4 *	1.4
1000	cytotoxicity	1.4 *	2.0 *

Table 7b - OECD reference NM causing significant TNF-α induction (x-fold of NC; NC: pg/mL) in PCLuS at non-cytotoxic concentrations

NM; μg/mL	NM-100 TiO$_2$	NM-200 SiO$_2$	NM-211 CeO$_2$	NM-212 CeO$_2$	NM-402 MWCNT
NC	26.2 = 1.0 [a]	29.9 = 1.0	22.7 = 1.0 [b]	33.7 = 1.0 [a]	18.5 = 1.0 [a]
10	1.5	1.5 [a]	2.3	1.4	1.4
100	2.1 *	2.0 *	3.5 *	2.7 *	1.8 [c] *
1000	cytotoxicity	2.0 *	cytotoxicity	cytotoxicity	cytotoxicity

Table 7c - OECD reference NM causing significant CINC1 (IL-8) induction (x-fold of NC; NC: pg/mL) in PCLuS at non-cytotoxic concentrations

NM; μg/mL	NM-101 TiO$_2$	NM-103 TiO$_2$	NM-104 TiO$_2$	NM-211 CeO$_2$	NM-212 CeO$_2$	NM-401 MWCNT	NM-402 MWCNT
NC	6200 = 1.0	52 800 = 1.0 [a, c]	15 800 = 1.0	21 800 = 1.0 [a]	25 700 = 1.0 [a]	43 200 = 1.0 [b]	26 100 = 1.0 [a]
10	1.8 *	0.9	0.8	0.9 [a]	0.9	1.7 [a]	0.8
100	cytotoxicity	0.9	2.3 *	1.8*	1.6 *	2.4 *	1.4 *
1000	cytotoxicity	1.5 *	2.3 [a] *	cytotoxicity	cytotoxicity	cytotoxicity	cytotoxicity

Table 7d – OECD reference NM causing significant MCP-1 induction (x-fold of NC; NC: pg/mL) in PCLuS at non-cytotoxic concentrations

NM; [μg/mL]	NM-103 TiO$_2$
NC	4200 =1.0
10	1.0 [a]
100	1.1
1000	2.0 [d] *

Table 7e - OECD reference NM causing significant M-CSF induction (x-fold of NC; NC: pg/mL) in PCLuS at non-cytotoxic concentrations

NM; [μg/mL]	NM-100 TiO$_2$	NM-101 TiO$_2$	NM-104 TiO$_2$	NM-211 CeO$_2$	NM-212 CeO$_2$	NM-401 MWCNT
NC	14.0 = 1.0	14.0 = 1.0	14.0 = 1.0	14.0 = 1.0	23.1 = 1.0 [b]	19.1 = 1.0
10	1.8 *	2.3 [a] *	1.1	1.1	1.5	5.2 [a] *
100	2.6 *	cytotoxicity	1.4 [a]	3.6 *	2.5 *	4.5
1000	cytotoxicity	cytotoxicity	2.0 [a] *	cytotoxicity	cytotoxicity	cytotoxicity

Table 7f - OECD reference NM causing significant OPN induction (x-fold of NC; NC: pg/mL) in PCLuS at non-cytotoxic concentrations

NM; [μg/mL]	NM-100 TiO$_2$	NM-101 TiO$_2$	NM-104 TiO$_2$	NM-200 SiO$_2$	NM-211 CeO$_2$	NM-212 CeO$_2$
NC	200 = 1.0 [b]	500 = 1.0	4500 =1.0 [b, c]	2000 = 1.0 [c]	500 = 1.0	800 = 1.0 [a]
10	8.2 [a] *	3.0 *	0.6	1.3 [a]	1.7 [a]	1.0 [a]
100	12.9 *	cytotoxicity	1.1	1.8 *	2.9 *	1.5 *
1000	cytotoxicity	cytotoxicity	1.8 *	2.3 *	cytotoxicity	cytotoxicity

- NC: negative control (DMEM/F-12)
- Cytokine assays:
  NC — mean concentration of duplicate testing (pg/mL); set as 1.0
    IL-1α determined in cell lysate
    TNF-α, CINC1 (IL-8), MCP-1, M-CSF and OPN determined in PCLuS supernatant

Test substance effects — x-fold increase relative to the NC
- a: CV% > 20%; b: CV% > 50%
- c: NC did not meet respective acceptance criterion
- *Statistical significance (p ≤ 0.05) in trend analysis

Table 8
Overview of in vitro effects of 16 OECD reference nanomaterials in PCLuS (details: see Footnote and Tables 3–7).

		Tissue Destruction	Cytotoxicity*	Apoptosis	Oxidative Stress**	Inflammation**	No Effect
TiO₂, anatase	NM-100		500	500		10	
anatase	NM-101		100		10	10	
anatase	NM-102				1000		
rutile	NM-103					1000	
rutile	NM-104				1000	100	
rutile-anatase	NM-105						10 -1000
ZnO	NM-110	10					
	NM-111	10					
SiO₂	NM-200			500		100	
	NM-203						10 -1000
CeO₂	NM-211		1000			100	
	NM-212		1000			100	
Ag	NM-300K	50					
MWCNT	NM-400						10 -1000
	NM-401		1000		500	10	
	NM-402		500			100	

The lowest test substance concentrations (μg/mL) at which the respective effects were observed are noted.
* Significant cytotoxicity at test substance concentrations not causing tissue destruction
** Significant oxidative stress or inflammation at test substance concentration causing neither tissue destruction nor cytotoxicity

TiO₂ NM-101 and NM-104 (both: IL-1α, CINC1 (IL-8), M-CSF, and OPN) and both CeO₂ NM-211 and NM-212 (both: TNF-α, CINC1 (IL-8), M-CSF, and OPN) induced all three types of cytokines at non-cytotoxic concentrations, i.e. the pro-inflammatory cytokines modulating immune reactions, the chemokines inducing infiltration of inflammatory cells into the lung tissue, and the cytokines inducing proliferation of hematopoietic or sessile cells. TiO₂ NM-100 only induced TNF-α, M-CSF, and OPN, whereas TiO₂ NM-103 induced CINC1 and MCP-1, thereby being the only NM to induce MCP-1. SiO₂ NM-200 induced IL-1α, TNF-α, and OPN. MWCNT NM-401 induced CINC1 and M-CSF and NM-402 TNF-α and CINC1 (Table 7a–f and SI Tables S6–S11).

Test substance-specific observations taking into account histopathological evaluations of the PCLuS test system

An overview of the in vitro effects induced by the 16 OECD reference nanomaterials evaluated in the PCLuS test system is provided in Table 8. In the following, these effects are compared to the outcome of the histopathological evaluations.

The ion shedding nanomaterials, ZnO NM-110 and NM-111, and Ag NM-300K, induced considerable tissue destruction, as evidenced by severe loss of protein content in the BCA protein assay. Presumably, the uncoated ZnO NM-110 was slightly more toxic than its coated counterpart, since ZnO NM-111 did not induce significant effects at all test substance concentrations. Surprisingly in histopathology, ZnO NM-111-exposed lung slices did not show any signs of cytotoxic effects, but in the alveolar lumen in a non-concentration dependent manner. Most likely, this observation is an artifact caused by technical problems. In the histopathological evaluation of those lung slices exposed to Ag NM-300K and the silver dispersant NM-300K DIS, condensed nuclei and vacuolated cytoplasm of lung cells were observed, an indication of autophagy, and possibly apoptosis, with more severe changes induced by silver than its dispersant (Table 10 and Fig. 1).

Among the less- or insoluble metal oxide nanomaterials, pigmentary (non-nano) anatase NM-100 and anatase NM-101 were the most toxic TiO₂ NMs evaluated in the present study, by inducing significant cytotoxicity combined with cytokine induction at non-cytotoxic concentrations and, in the case of NM-100, caspase-3/-7 activation,

and, in the case of NM-101, increased GSH concentrations. Both CeO₂, NM-211 and NM-212, showed similar levels of toxicity, inducing significant cytotoxicity and identical cytokine patterns, i.e. TNF-α, CINC1, M-CSF, and OPN at non-cytotoxic concentrations. Histopathological evaluation of the lung slices exposed to these test substances revealed nanoparticles, seen as agglomerates of black, round particles, in macrophages and free in the alveolar lumen, but no signs of cellular death (Table 10 and Fig. 2a, presenting NM-102 agglomerates in the alveolar lumen, and Fig. 2b, presenting NM-102 particles taken up into macrophages).

SiO₂ NM-200 significantly activated caspase-3 and -7, however without concurrent cytotoxicity. In histopathological evaluation of NM-200-exposed PCLuS, single cell necrosis and eosinophilic material in alveoli were observed, whereas the almost translucent SiO₂ nanoparticles were hardly to be seen with light microscopy (Table 10 and Fig. 3). Oxidative stress, as determined by increased GSH levels, but no cytotoxicity, was observed for anatase TiO₂ NM-102 (which induced none of the cytokines) and for rutile TiO₂ NM-104, which further induced all three types of cytokines. Histopathological evaluation of PCLuS exposed to these substances resembled those of the cytotoxic substances, however with slightly lower grades of severity at the higher concentrations. Finally, TiO₂ NM-103 only induced cytokines (i.e. CINC1 and MCP-1), and TiO₂ NM-105 and SiO₂ NM-203 induced no significant effects in any of the assays.

The three different multi-walled carbon nanotubes included in the present study differed considerably in the effects they elicited. Whereas MWCNT NM-400 did not induce any significant effects in any of the assays, NM-401 and NM-402 caused significant cytotoxicity, NM-401 also increased GSH levels and both NM-401 and NM-402 further induced cytokines, i.e. CINC1 and M-CSF (in the case of NM-401) or TNF-α and CINC1 (in the case of NM-402). In histopathology, none of the MWCNT-treated PCLuS showed any sign of cell alteration, but carbon nanotubes observable as fibrous structures in the alveolar macrophages and in the alveolar lumen (Table 10 and Fig. 4).

In comparison to the histopathological findings of the test substance-treated lung slices, in PC(Triton X100)-treated PCLuS considerable cell lysis had occurred resulting in a loss of cell nuclei and cellular structures (Fig. 5). In the SiO₂ NM-203 and CeO₂ NM-212 test runs, however, histopathological evaluation of the Triton X-100-treated lung slices did not reveal any changes in cell morphology. These observations might point to technical problems for these two test runs (Table 10). Finally, histopathological evaluation of the NC, i.e. the PCLuS treated only with cell culture medium (DMEM), revealed intact alveoli with no evidence of foreign particles present either in the lumina or cells (Fig. 6).

Discussion

Inherent sensibility of the PCLuS test system

For in vitro or ex vivo test systems to become applicable for routine regulatory testing, a test protocol has to be compiled that is sufficiently straightforward to enable reliable test substance screening at a sufficiently high throughput. In the present study such a test protocol for the PCLuS test system, using uniform 24-hour submerse test substance exposure, has been evaluated. Furthermore, the same test substance concentrations of 10 to 1000 μg/mL were consistently applied for all assays, which were selected to cover relevant NM toxicity pathways, i.e. cytotoxicity, apoptotic reactions, oxidative stress, and inflammatory reactions. Standardization of test protocols, however, can prove very challenging during in vitro test development (Fentem et al., 1995), and the acceptance criteria and measures set up to verify test result reliability and reproducibility reveal a number of limitations of the PCLuS test system as it was used in the present study.

Test result reliability and reproducibility can be impaired by limitations inherent to the tissue slice test system itself, arising both from the preparation and the handling of the PCLuS. A crucial,

Table 9
Fulfillment of acceptance criteria (AC) and reproducibility of test results in the protein, WST-1, GSH, caspase-3/-7, and cytokine assays (numbers of NC and PC not meeting the AC and numbers of measurements with CV% >20% and >50% as compared to reported mean intra- and interassay variabilities).

Assay	NC-related AC**	No. of NC not meeting AC	PC-related AC**	No. of PC not meeting AC	Total no. of measurements (incl. NC & PC)*	No. of measurements with CV% >20% /of which >50%	Reported mean intra-assay variability (CV%)***	Reported mean inter-assay variability (CV%)
	Mean NC		Mean PC					
Total protein	≥0.4 OD	0/17	≤50 μg/mL	0/17	119	7/0	Not available	Not available
WST-1	≥0.5 OD	1/13	≤10% relative to NC	0/13	91	5/1	<4.2 a	Not available
Caspase-3/-7	≤40% relative to PC	2/13	≥60 000 RLU	3/13	91	13/0	Not available	Not available
GSH	≥8000 RLU	5/13	≤30% relative to NC	1/13	81	20/3	not available	not available
IL-1α	<1.0 ng/mL	4/12	No PC	Not applicable	41	9/1	Not available [6/12]	Not available
TNF-α	<50 pg/mL	1/12				15/3	8.6 b [10]	13.5 b
CINC1 (IL-8)	<40 ng/mL	2/12				10/3	<7.5 c [3/14]	<6.5 c
MCP-1	<5 ng/mL	0/12				6/2	12.9 d [8/10]	8.1 d
M-CSF	<30.0 pg/mL	2/12				10/4	<9 e [3/6]	<9 e
OPN	<1.5 ng/mL	4/12				11/10	<4 f [2]	<6.6 f

NC: negative control (DMEM/F12); PC: positive control; AC: acceptance criterion; TR: test result; CV%: coefficient of variation; RLU: relative luminescence unit
PC: WST-1 assay: 0.1% Triton X-100; caspase-3/-7 assay: 0.5 μM staurosporine; GSH assay: 10 mM DL-buthionine-[S,R]-sulfoximine (BSO); no PC in the cytokine assays.
In the protein, WST-1, and caspase-3/-7 assays, the total number of test substances equals 7 times (i.e. 5 test substance concentrations plus NC and PC) the number of test substances included in the assay (i.e. 17 and 13 test substances). The total number of test results evaluated in the GSH assay equals the total number of test results evaluated in the WST-1 minus 10 test substance concentrations with significant cytotoxicity in the WST-1 assay. In the cytokine assays, the maximum number of test results was 41, i.e. 12 NM (TiO₂ NM-105 also excluded), no PC, only non-cytotoxic test substance concentrations, and only 3 test substance concentrations.
a: see Peskin and Winterbourn (2000)
b: Test kit leaflet for the flow cytomix simplex Kit rat TNF-alpha (available at: http://www.bendermedsystems.org/bm_products/MAN/8622FF.pdf)
c: Test kit leaflet for the Quantikine rat CINC-1 ELISA (available at: http://www.rndsystems.com/Products/RCN100)
d: Test kit leaflet for the Flow cytomix simplex Kit rat MCP-1 (available at: http://www.bendermedsystems.org/bm_products/MAN/8631FF.pdf)
e: Test kit leaflet for the Quantikine Mouse M-CSF ELISA (available at: http://www.rndsystems.com/Products/MMC00)
f: Test kit leaflet for the Quantikine Mouse Osteopontin ELISA (available at: http://www.rndsystems.com/Products/MOST00)
  * Acceptance criteria (adapted from Lauenstein et al., 2012). Due to the strong cytotoxic effect of Triton X-100, in the WST-1 assay, the PC-related AC only confirms that cell lysis has occurred.
  ** Maximum number of test results
  *** Figures in square brackets relate to own measurements in the PCLuS test system during standard curve determination (see Table S1)

fundamental step when performing tests with precision-cut lung slices is the preparation of the tissues. The cutting of the slices is an insult that can lead to cellular reactions, which might distort test results. Wohlsen et al. (2003) address a number of potential tissue-related problems when using PCLuS to measure small airway responses, such as cellular changes induced by agarose instillation into the lung, pre-contraction of the airways, and – in regard to the uniform quality of the tissue slices – airways of different diameters being present in different slices. Assay-specific variations in the NC measurements indeed point to a certain degree of tissue damage due to the cutting or handling of the lung slices even though these were performed with utmost care. They further indicate that a certain degree of biological variability is to be expected in PCLuS test systems. Recently, it has been suggested to delay exposing PCLuS to test substances until 48 h after preparing the slices to reduce responses caused by the slicing procedure itself (Behrsing et al., 2013). Under the testing conditions of the present study, however, cell viability

Table 10
Histopathological evaluation of PCLuS treated with OECD reference nanomaterials.

OECD reference No. and test substance	Positive control	Grade of severity at respective concentration [μg/mL]			Observation
		10	100	1000	
NM-100 TiO₂	P	2	4	4*	Particles in macrophages and free in alveolar lumen
NM-101 TiO₂	P	1	2	4	Particles in macrophages and free in alveolar lumen
NM-102 TiO₂	P	1/1	1/2	1/3–4	Particles in macrophages and free in alveolar lumen
NM-103 TiO₂	P	1/1	1/2–3	1/3–4	Particles in macrophages and free in alveolar lumen
NM-104 TiO₂	P	1/2/1	2/2	2/4	Particles in macrophages and free in alveolar lumen
NM-111 ZnO	P	1	1	1/1–2	Particles in macrophages and free in alveolar lumen
NM-200 SiO₂	P	1	2	3/2–3	Single cell necrosis and eosinophilic material in alveoli
NM-203 SiO₂	nad**	nad	nad	1/1	Particles in macrophages and free in alveolar lumen
NM-211 CeO₂	P	1	2–3	4	Particles in macrophages and free in alveolar lumen
NM-212 CeO₂	nad**	1	1/1	2/3	Particles in macrophages and free in alveolar lumen
NM-300K Ag < 20 nm	P	1	2/1–2	4/2	Condensed nuclei, vacuolated cytoplasm; particles in macrophages and free in alveolar lumen
NM-300KDIS Ag dispersant	P	nad	1–2/1	4/1	Vacuolated cytoplasm; condensed nuclei; particles free in alveolar lumen
NM-401 MWCNT	P	1/1	1/3	1/4	Particles in macrophages and free in alveolar lumen
NM-402 MWCNT	P	1/1	1/2–3	1/4	Particles in macrophages and free in alveolar lumen

The numbers categorize the severity of the respective observation:
Grade 1: minimal; 2: slight, mild; 3: moderate; 4: marked, severe; 5: massive, extreme
P: histopathological findings present
NC: negative control (DMEM/F-12); PC: positive control (0.1% Triton X-100)
  * Tested at 840 μg/mL, i.e. the dispersed concentration calculated for NM-100
  ** nad = nothing adverse detected; histopathological evaluation points to technical problems relating to test sample with positive control
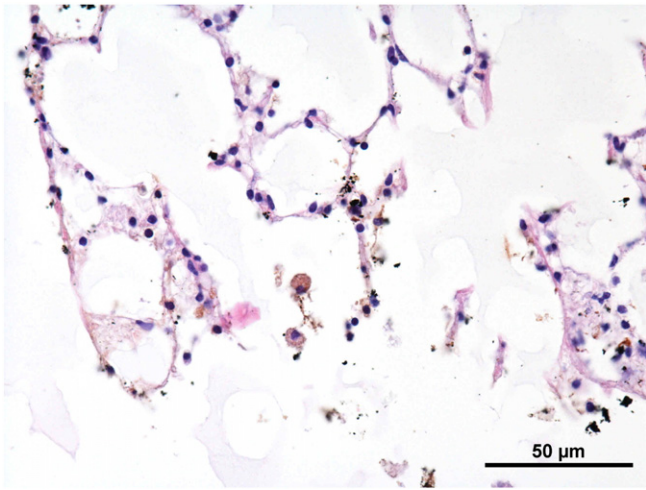
Fig. 1. PCLuS treated with 1000 μg/mL Ag NM-300K: NMs in macrophages and in alveolar lumen; cells: condensed nuclei and vacuolated cytoplasm.
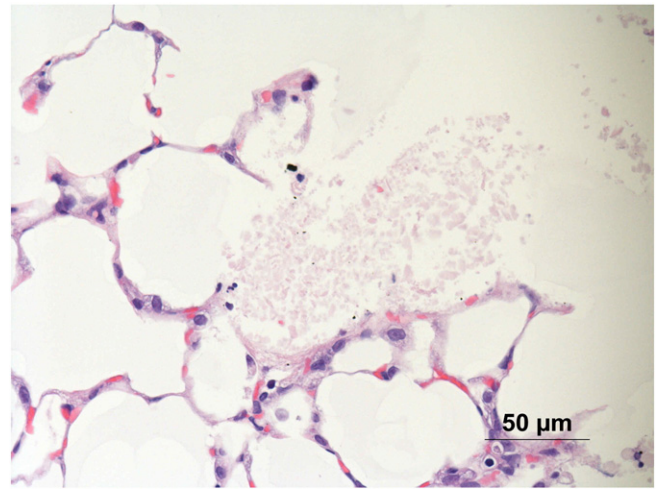

Fig. 3. PCLuS treated with 1000 μg/mL SiO₂ NM-200: Cell necrosis and eosinophilic material in alveoli, translucent SiO₂ NMs hardly to be seen.
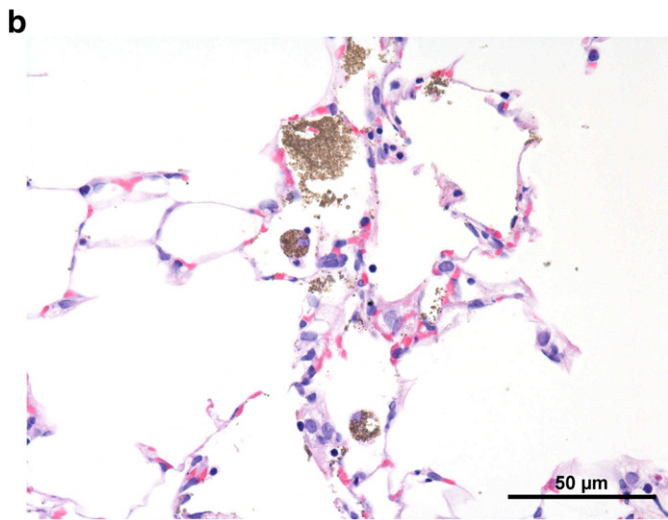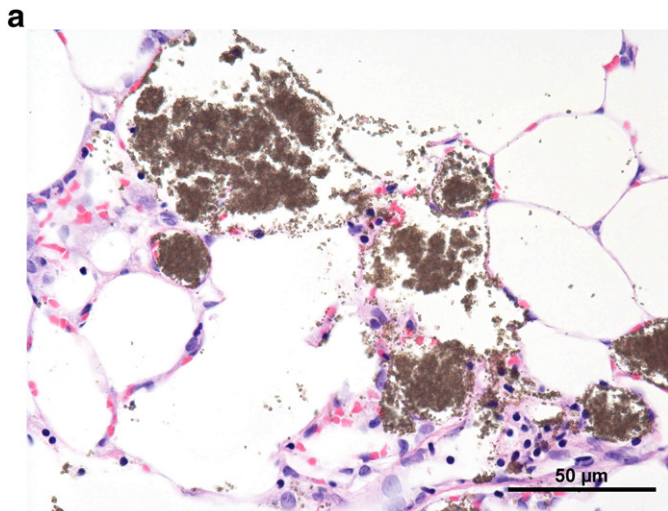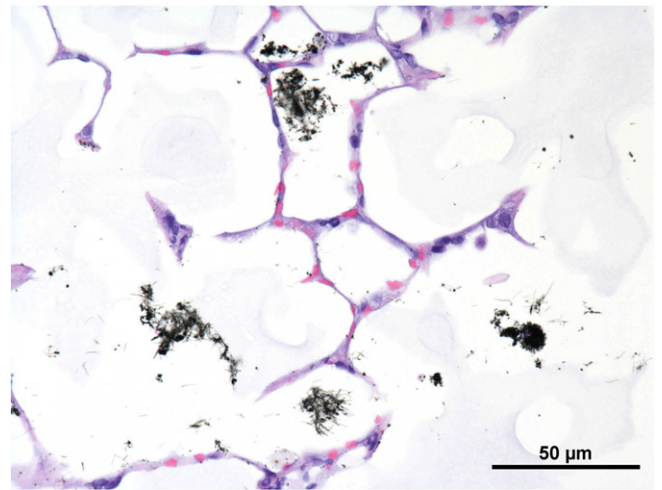

Fig. 4. PCLuS treated with 1000 μg/mL MWCNT NM-401: NMs in macrophages and in alveolar lumen.

Fig. 2. a: PCLuS treated with 1000 μg/mL TiO₂ NM-102: (Agglomerated) NMs in macrophages and in alveolar lumen. b: PCLuS treated with 1000 μg/mL TiO₂ NM-103: (agglomerated) NMs in alveolar lumen and additionally in macrophages.
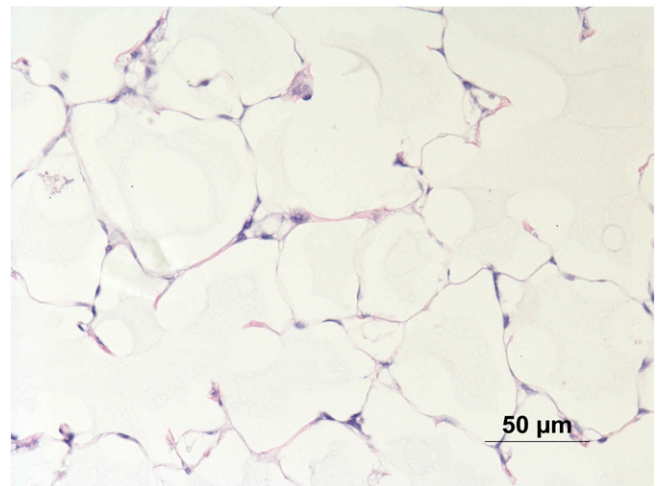
Fig. 5. PCLuS treated with 0.1% Triton X-100: Considerable cell lysis resulting in a loss of cell nuclei and cellular structures.
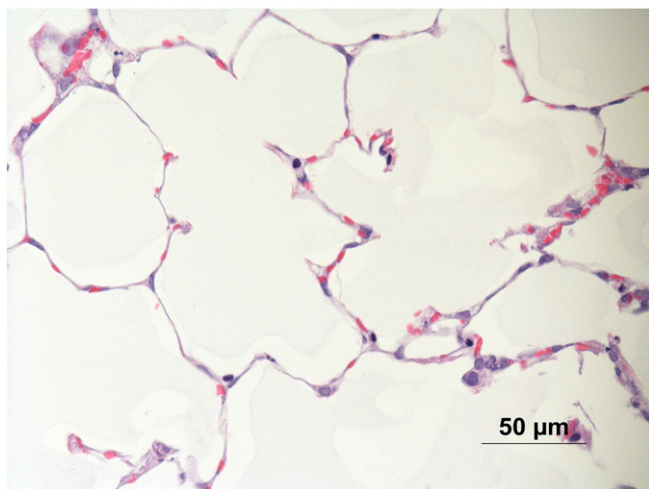
Fig. 6. PCLuS treated only with cell culture medium (DMEM, i.e. negative controls): Intact alveoli, no foreign particles to be detected.

of the PCLuS test system was best during the first 24 h after preparation of the slices. Therefore the test substances were applied without recovery period after the cutting procedure.

Whereas the uniform quality of monolayer cell culture test systems can be established, e.g. by determining cell confluence using light microscopy, the quality of tissue slices can only be assessed indirectly. Frequently, total protein content of the tissue slices – as a quantifiable parameter relating to the cell numbers – is used to determine standard quality and to rule out technical problems during to their preparation (Henjakovic et al., 2008; Switalla et al., 2010a,b).

The BCA protein assay, applied in the present study to determine total protein mass, requires lysating the slices. Since only the WST-1 assay does not in itself require lysating the slices, the BCA protein assay therefore could only be performed upon completion of this assay, but not to verify the quality of the slices used in the caspase-3/-7, GSH, or cytokine assays. While all of the slices tested in the BCA protein assay were of acceptable thickness, the range of total protein contents measured throughout the entire study (i.e. between 159 μg/mL for the NC of TiO$_2$ NM-105 and 422 μg/mL for the NC of ZnO NM-111) suggests that in the respective test runs test substances at identical concentrations were in fact applied to differing numbers of cells. To address tissue variability (at least in the WST-1 assay), the absorbance values calculated in this assay were related to the total protein contents of the tissue slices.

Test result reproducibility and endpoint-specific observations

Coefficients of variation exceeding 20% were observed for mean test results in all assays, however in different frequencies. A number of reasons can be put forward for this: Inconsistencies in NM dispersion do not seem to be the likely main cause since CV% values exceeding 20% were also observed for the negative and positive controls. The BCA protein and WST-1 assays were the most reproducible assays since they fulfilled the respective NC- and PC-related AC and had overall satisfactory coefficients of variation. (It cannot be determined whether the higher CV% values in the WST-1 assay recorded for TiO$_2$ NM-103 at three different test concentrations were caused by technical problems during test substance sampling, tissue slice preparation, or assay performance.)

In contrast, CV% values exceeding 20% were recorded frequently in the GSH assay (23 of 81 measurements). GSH depletion is likely to be a very sensitive endpoint that is already affected by the preparation of the lung slices as revealed by the number of NC with reduced GSH levels (i.e. that did not meet the respective NC-related AC). Furthermore,

in vitro glutathione levels have been reported to be very low to begin with, making GSH difficult to detect. Additionally, nanoparticles have been observed to trigger the active export of intracellular glutathione by increasing the activity of the ATP-dependent MRP/1 efflux pumps, which in return leads to increased ROS production and cellular apoptosis (Seiffert et al., 2012; Stone et al., 2009). Increased GSH levels induced by a number of NMs in the present study might be an indication of late oxidative stress reactions that occur as a detoxifying defense mechanism after the initial GSH decrease (Lin and Yang, 2007).

Consistent with the findings of the present study, also other in vitro studies have highlighted IL-8 as an important cytokine to detect inflammatory reactions caused by different types of NMs (Donaldson et al., 2008; Feltis et al., 2012; Hackenberg et al., 2011; Kermanizadeh et al., 2013). Additionally, zinc nanoparticles of different shapes and sizes have been observed to induce TNF-α (Roy et al., 2011) and MCP-1 (Gojova et al., 2007), and P-25 TiO$_2$ NMs (21 nm) were found to induce IL-1, IL-6, IL-8, and TNF-α in vitro (Park et al., 2008).

However, large variations of the PCLuS test results were observed for the six different cytokine assays. Most likely, this was due to the different affection of the lung cells during the cutting and handling procedure, as confirmed by high CV% values in the negative controls. For those cytokines that were induced by a number of NMs (TNF-α, CINC1 (IL-8), M-CSF, and OPN), test result reproducibility was mediocre. Cytokine inductions in PCLuS cannot be expected to be as pronounced as immune reactions in vivo, since they are restricted to the piece of tissue available in the ex vivo test system and, e.g., attraction of immune cells from the blood to the site of inflammation is not possible. Therefore, cytokines are not considered to be core parameters in testing NM toxicity in PCLuS.

As regards caspase-3/-7 activation, only two test substances (TiO$_2$ NM-100 and SiO$_2$ NM-200) elicited a statistically relevant effect. Nevertheless, the observation that the most pronounced effects in the caspase-3/-7 assay frequently occurred at the second highest, or even lower, test substance concentrations possibly point to the need to further optimize the PCLuS apoptosis assay protocol. Wilhelmi et al. (2012) cautioned against potential artifacts when testing nanomaterials in the caspase assay and ruled out possible false positive results by cell-free testing of all materials. This measure is also recommended by the supplier of the Caspase-Glo® 3/7 assay kit (http://www.promega.de/~/media/Files/Resources/Protocols/Technical%20Bulletins/101/Caspase-Glo%203%207%20Assay%20Protocol.pdf).

Furthermore, in podocytes, 5 and 10 mg/mL human albumin, the dispersing agent used in the present study, induced dose-dependent caspase-3-/-7-activation and apoptosis (Okamura et al., 2013). Therefore also albumin-addition to the culture medium might cause false positive results. In contrast in the present study, apart from SiO$_2$ NM-200, there was an overall lack of apoptotic effects.

Wilhelmi and co-authors found absorption measurements to be wavelength-dependent in the caspase assay. They recorded ZnO and TiO$_2$ nanoparticles to be especially prone to decrease the luminescent signal in the caspase-3/-7 assay and further reported high inter-experimental variability of this assay. In the present study, unlike the effect induced by TiO$_2$ NM-100, the caspase-3 and -7 activation elicited by SiO$_2$ NM-200, did not correspond with cytotoxic cell death at the tested concentrations. However singular cell necrosis and eosinophilic material were observed in histopathology at the highest test concentrations. Caspase-3 activation without cell death has been reported to occur in CD8 + T cells upon antigen presentation (McComb et al., 2010). Likewise, cellular infections have been reported to induce caspase-1 activating inflammasomes triggering the maturation of pro-inflammatory cytokines to engage in innate immune defenses and pyroptotic cell death (Lamkanfi, 2011; Schroder and Tschopp, 2010). However, such immune reactions are very unlikely to have occurred in the ex vivo lung slices. It remains to be determined whether longer exposure times or longer post-exposure observations times would have resulted in apoptotic cell death.

The LDH release assay, originally under consideration for inclusion in the present study, was omitted after nanomaterial interferences with the assay dye could not be prevented for all NMs as determined by NM-reagent interferences in cell-free dispersions. Recently, however, also an interference of P-25 TiO$_2$ NM with the formazan dye used in the MTT assay has been reported (Lupu and Popescu, 2013). For test substance concentrations exceeding 50 μg/mL, this resulted in false viability increases of up to 14%. Further investigations are required to determine whether the cytotoxicity recorded for TiO$_2$ NM-100 and NM-101 in the present study has been influenced to some extent by such NM-dye interactions. Recently however, Guadagnini et al. (2013) have not found two different SiO$_2$ NMs (15-30 and 25–50 nm, respectively (TEM and DLS)), or TiO$_2$ NM-105 (15–60 nm (TEM); 101 and 278 nm (bimodal size distribution in DMEM-F12-HAM culture medium; DLS)) to interfere with the reagents of the WST-1 assay.

Limitations of the available positive controls

Positive controls serve to monitor the inducibility of the PCLuS in the respective assays. However, for the cytokine assays LPS was discarded as positive control because of poor reproducibility of test results resulting in frequent failure to meet the respective PC-related AC. Feltis et al. (2012) also found the quality of LPS to be variable when using it as a positive control to investigate ZnO NM effects on THP-1-derived macrophage cultures. Additionally, as mentioned above, the mode of action of LPS on inflammatory cells differs from that of NMs. In the BCA protein and WST-1 assays (as well as in histopathological evaluation), the effects caused by the PC Triton X-100 possibly were too detrimental to calibrate mild or moderate effects caused by NMs. This lack of suitable positive controls is an obstacle standing in the way to the optimization of in vitro assays.

In regard to those assays where test results are recorded relative to the NC or PC (i.e. caspase-3/-7 activation and GSH depletion/increase), the difference between the effects measured for the NC and the PC must be sufficiently high to allow for a meaningful assignment of concentration-dependent test substance reactions. Overall in the caspase-3/-7 assay, test substance-induced enzyme activation was not considerably higher than caspase activation in the NC. Again, this might point to a certain degree of pre-treatment tissue damage in the lung slices. It might also point to the low apoptotic activity of the NMs tested in relation to the much more pronounced effects of the positive control staurosporine.

Test substance exposure duration and exposure type

In the caspase-3/-7 assay, the most pronounced effects oftentimes were not recorded at the highest test substance concentration. Significant effects observed in the GSH assay only related to increased but not reduced GSH levels. Additionally, IL-1α, an important pro-inflammatory marker, was hardly ever increased to significant levels. All of these findings might be an indication that the early cellular effects investigated in these assays might already have passed their peak at the time of investigation.

As regards a timeline for the progression of apoptotic reactions in in vitro cell culture test systems, Hussain et al. (2010) found caspase-3/-7 activation upon exposure of 20 μg/cm^2 TiO$_2$ NM (12 nm, TEM) to 16HBE14o- cells to reach a maximum after 2 h. After 30 min of exposure, ROS production, lipid peroxidation, and lysosomal membrane destabilization were induced, leading to cathepsin B release and caspase-8 activation after 1 h, and caspase-3/-7 activation after 2 h (Hussain et al., 2010). In RAW 264.7 macrophages, non-nano crystalline silica DQ12 and amorphous SiO$_2$ nanoparticles dose-dependently (10–80 μg/cm^2) induced caspase-3/-7 after 6-hour treatment, which was significant for DQ12 at 80 μg/cm^2. After 24-hour treatment, however, increases in caspase-3/-7 activation were not significant, and

ZnO nanoparticles were even found to reduce caspase activities below those of untreated cells (Wilhelmi et al., 2012).

Different nanoparticle exposure times have also been selected to detect different cytokines in vitro. Feltis et al. (2012) exposed human THP-1 cell-derived macrophages to ZnO nanoparticles for 20 h before conducting extensive cytokine analysis. Heng et al. (2011a) measured TNF-α in primary murine dendritic cells after 6-hour exposure to ZnO nanoparticles. Duffin et al. (2007b) treated A549 cells to nanoparticle carbon black and nanoparticle TiO$_2$ for 4 h before measuring IL-8 in the culture supernatants. When applied to cultured human aortic endothelial cells, ZnO nanoparticles increased ICAM-1 mRNA levels after 1–2 h which then remained at an elevated level, whereas IL-8 and MCP-1 mRNA expression peaked at 2 h before decreasing to considerably lower levels (Gojova et al., 2007).

Overall, the extent of endpoint-specific effect is dependent upon the type of test system chosen. For instance, IL-8 concentrations induced by TiO$_2$ NM and diesel exhaust particles were lower in triple cell co-cultures composed of human A549 cells, macrophages, and dendritic cells, than the expected values calculated from the respective monocultures of each of the cell types (Müller et al., 2010). TNF-α concentrations, on the other hand, were higher in the triple cell co-cultures, revealing that the interplay of different lung cell types can substantially modulate nanoparticle effects (Müller et al., 2010).

Exposure times found suitable for monolayer cell culture systems are not per se also appropriate for tissue culture systems, since the test substances are exposed to different cellular assemblages. For practical reasons, a uniform exposure time for the different assays applied in the PCLuS test system is desirable. As these specifications reveal, adaptations of the test substance exposure times in the caspase-3/-7, GSH, and, possibly, some of the cytokine assays might improve the validity of these assays.

Finally, also the question whether application of the test substances dispersed in solution adequately reflects the situation in vivo is a matter for further investigation. It has been suggested that culturing PCLuS at an air-liquid interface might more closely resemble in vivo exposure (Herzog et al., 2013; Switalla et al., 2010b). However, this technique is not yet well suited for high-throughput screening assays.

Dose metrics and dosimetry

For adherent cell cultures, it has been recommended to relate nanoparticle mass to the culture dish surface area or to the number of cells per unit surface area of the culture dish (Heng et al., 2011b; Rushton et al., 2010; Stone et al., 2009). Due to the heterogeneous tissue structure of the lung slices used as test system in the present study, the cell numbers per unit surface area of the culture dish are not uniform. Therefore, in spite of the limitations of expressing NM concentrations in terms of mass per unit volume (or mass per unit well surface area), this dose metric was considered most suitable for the PCLuS test system.

In regard to the specific nanoparticle dispersion dynamics, calculations directly relating in vitro test substance concentrations to in vivo target tissue doses, i.e. lung burden, over a given exposure time are not adequate for nanoparticles (Teeguarden et al., 2007). In contrast to soluble chemicals, nanoparticles can settle, diffuse, and aggregate differently according to their size, density, and surface physico-chemistry, and also depending on the properties of the culture media applied. Gravitational particle settling, diffusion, and agglomeration are processes that are expected to significantly affect the cellular dose and hence the cellular effect of the NMs (Hinderliter et al., 2010; Teeguarden et al., 2007). As a result, slow or non-settling particles are more likely to evade common in vitro measures of biological responses, such as cell death and protein expression as investigated within the time frame of typical in vitro experiments (Teeguarden et al., 2007). Given their size, the regional deposition of NMs in the respiratory tract in vivo is mainly governed by diffusion (Landsiedel et al., 2012; Oberdörster, 2009).

Calculations of the effective dosages applied in the present study, via ISDD model for the well-dispersed NMs (for which diffusion is the predominant parameter) and directly via AUC for the strongly agglomerated NMs (for which sedimentation is the predominant parameter), revealed vast differences in the effective dosages between different NMs. They further indicated that the highest in vitro test substance concentrations exceeded the highest in vivo dosage previously applied in rat short-term inhalation studies.

Whereas the broad dose range up to 1000 μg/mL was selected in the present study to ensure eliciting the in vitro effects under investigation, thereby determining inducibility of the PCLuS test system, further investigations are required to adequately adjust in vitro test substance concentrations to the differing diffusion and sedimentation properties of different NMs and also to align in vitro dosages to in vivo dosages.

Particle characteristics influencing particle effects

Physico-chemical properties of nanomaterials that have been recognized to influence their inhalability, deposition efficiency, and toxicology are their airborne and hydrodynamic size, size distribution, shape (and aspect ratio), their state of agglomeration, surface properties and functionalization (surface area, porosity, charge, reactivity, chemistry/coatings, contaminants), as well as solubility and crystallinity (Kuempel et al., 2012; Nel et al., 2013a; Oberdörster, 2009; Oberdörster et al., 1994; Rodriguez-Yanez et al., 2013; Zhu et al., 2013). Also in in vitro cytotoxicity assays, particle size, surface chemistry and coating, as well as chemical composition have been recognized as key determinants of nanoparticle adverse effects (Feltis et al., 2012; Horev-Azaria et al., 2011; Kroll et al., 2011). For nanotubes and fibers, the number concentration of specific sized structures has been associated with inflammatory effects (Donaldson et al., 2010). Furthermore, at equivalent cytotoxic loads, smaller nanoparticles induced greater cellular immune responses (Feltis et al., 2012).

As regards chemical properties of the NM test substances applied in the present study, the ion shedding ZnO and Ag NMs induced the strongest toxic effects in the PCLuS test system. Regarding those NMs inducing moderate cytotoxicity, anatase TiO$_2$ NMs elicited stronger effects than rutile or rutile-anatase NMs of the same chemical composition, since two of the anatase TiO$_2$ NM (NM-100 and NM-101) caused cytotoxicity (with corresponding caspase-3/-7 activation or GSH increase) and the third one oxidative stress (NM-102), which was also recorded for rutile NM-104, whereas rutile-anatase NM-105 did not cause any adverse effects in any of the assays performed (no cytokine assays were performed for NM-105) and rutile NM-103 only inflammation. Other in vitro studies have also recorded higher cytotoxic potency for anatase TiO$_2$ NMs than for the rutile form (Johnston et al., 2009).

The hydrophobicity and hydrophilicity of NMs and the amount of phospholipids present on the NM surface are further important factors determining NM cellular uptake and intracellular distribution (Landsiedel et al., 2012; Zhu et al., 2013). Hydrophobic nanoparticles are generally poorly dispersed in biological fluids and culture medium. They tend to form aggregates or interact with hydrophobic residues of blood proteins or peptides to enhance their dispersion. Likewise, NMs taken up as aggregates or agglomerates tend to be less avidly cleared by the host, and residual nanoparticles in macrophages or stromal cells could last several months, thus possibly leading to cumulative toxicity (Zhu et al., 2013).

In the present study, bovine serum albumin-containing cell culture medium together with ultrasonication proved very effective in de-agglomerating carbon nanotubes, but also considerably reduced agglomeration for metal oxide nanomaterials (with very few exceptions; as compared to a phospholipid-containing dispersing agent; data not shown). Hydrophobic materials had a stronger tendency to agglomerate and a higher BSA affinity than the hydrophilic variants of the same

inorganic core thereby minimizing the total interfacial energy of the suspension.

Comparison of NM effects in the PCLuS test system to in vivo observations

To the best of the authors' knowledge, the present study is the first extensive evaluation of the applicability of the PCLuS test system for NM toxicity testing. Whereas all selected endpoints could be elicited, reflecting the spectrum of early cellular effects caused by NMs, the test protocol applied can only be considered preliminary, and the effects observed should not be regarded quantitative. Nevertheless, in the following, the results obtained with the PCLuS test system are compared to mechanisms of action recorded for the respective chemical types of NMs and to the results from in vivo rat inhalation toxcity studies published in the literature. Thereby, a first indication of the predictivity of the PCLuS test system is obtained. Since, however, the results from a rat PCLuS test system are only compared to data obtained in in vivo rat studies, extrapolations to possible effects in humans do not form part of this comparison.

Ion-shedding NMs that caused tissue destruction. The detrimental effects of ZnO nanoparticles on in vitro tissue integrity observed in the study at hand are well established. Mechanisms of action addressed for ZnO NMs are dissolution and release of heavy metal ions capable of ROS generation, inflammatory reactions inducing IL-8, IL-6, and TNF-α production, lysosomal damage, and cytotoxicity (Damoiseaux et al., 2011; Meng et al., 2009; Nel et al., 2009, 2013a). In vitro, dissolved Zn^{2+} ions have been reported to enter the mitochondria where they cause mitochondrial dysfunction, caspase activation, and cell apoptosis (Kao et al., 2012).

Also in vivo, ZnO NM effects are reported being caused by dissolved ions (Kuempel et al., 2012), as recorded by increased LDH levels in the bronchoalveolar fluid (BALF; Kao et al., 2012). Klein et al. (2012) found short-term inhalation exposure to 2.5 and 12.5 mg/m^3 Z-COTE® HP1 to increase inflammatory parameters in the BALF in a concentration-dependent manner. In pulmonary histology, reversible granulocyte infiltration and increases in alveolar macrophages were observed (Klein et al., 2012).

Mechanisms of action recognized for silver nanoparticles are dissolution and Ag + release inhibiting respiratory enzymes and ATP production, and causing ROS generation, as well as disruption of membrane integrity and transport processes (Damoiseaux et al., 2011; Meng et al., 2009; Nel et al., 2009, 2013a). Accordingly, the tissue destruction observed for Ag NM-300K in the present study was most likely caused by release of silver ions into the solution (Johnston et al., 2010).

In vivo studies determining Ag NM effects upon inhalation are scarce in the literature. After in vivo 4-hour whole body chamber inhalation exposure to 18–20 nm silver NM (76–750 μg/m^3; corresponding to 0.94–3.08 × 10^6 particles/cm^3), rats did not develop any adverse pulmonary effects within the 2-week observation period (Sung et al., 2011). However, Sung and co-authors do not report performing any histopathological evaluations that would allow comparing effects induced in vivo on the cellular level to in vitro cytotoxic events. Upon subchronic inhalation exposure (49–515 μg/m^3; corresponding to 0.6–3.0 × 10^6 particles/cm^3) to 15 or 18 nm Ag NMs, chronic alveolar inflammation and small granulomatous pulmonary lesions were observed (Sung et al., 2009) that did not regress in male, but in female rats (Song et al., 2013).

As discussed above, the highest concentrations applied in the PCLuS studies exceed the highest in vivo dosages. However, since tissue destruction was already recorded at concentrations of 10 and 50 μg/mL, the pronounced in vitro cytotoxicity of both ZnO and Ag NMs presumably reflect inflammatory effects in vivo that can be observed by cytological and histopathological evaluations. Chronic effects or reversibility of NM

effects during an in vivo observation period, on the other hand, cannot be mirrored in the PCLuS test system.

Metal oxide nanomaterials reported to be of moderate cytotoxicity. Mechanisms of action recognized for TiO_2 nanomaterials are glutathione depletion and toxic oxidative stress as a result of photoactivity and redox properties, protein fibrillation and cell membrane disruption leading to cell death (Damoiseaux et al., 2011; Meng et al., 2009; Nel et al., 2009, 2013a). In the present study, anatase NM-100 and NM-101 caused significant cytotoxicity at 500 and 1000 μg/mL (NM-101 additionally at 100 μg/mL). Three of the 4 NMs causing significant oxidative stress at non-cytotoxic concentrations were TiO_2 NMs, i.e. anatase NM-101 and NM-102 and rutile NM-104. Furthermore, NM-100 increased caspase-3/-7 activities at its cytotoxic concentrations. In the cytokine assays, CINC1 (IL-8) and M-CSF were induced by anatase and rutile TiO_2 NMs, whereas TNF-α was only induced by anatase TiO_2 NM-100.

In vivo adverse effects of TiO_2 NMs have been reported to be lung inflammation and, upon long-term exposure, pulmonary fibrosis, related to the total deposited or retained particle dose in the target respiratory tract region. For TiO_2 NMs, dose metrics related to adverse effects are surface area, volume, mass or number (by particle size fraction), with the dose–response relationship possibly being non-linear at low doses (Kuempel et al., 2012). In a rat short-term inhalation study (STIS; 5-day exposure period, 6-hour exposure/day), both nanoscaled (70% anatase/30% rutile, 20–30 nm, TEM; test substance concentration 100 mg/m^3) and pigmentary (non-nano) TiO_2 (200 nm, DLS; test substance concentration 250 mg/m^3) induced reversible mild neutrophilic inflammation and activation of macrophages in the lung (van Ravenzwaay et al., 2009). After exposing rats to 10 and 50 mg/m^3 TiO_2 NMs (25 nm, TEM) in the STIS, MCP-1, M-CSF, and OPN were significantly increased in a dose-dependent manner immediately after the final exposure. For the 10 mg/m^3, but not the 50 mg/m^3, dose group, these effects returned to control levels after a recovery period of 16 days (Ma-Hock et al., 2009a). Again, the PCLuS test system can only be expected to reflect early in vivo effects discernible on the cellular level, but neither progressive chronic reactions, nor the reversibility of effects.

Cytotoxic mechanisms reported for CeO_2 nanomaterials are inflammasome activation and protein aggregation and fibrillation (Nel et al., 2009, 2013a). In the PCLuS test system, the tested CeO_2 NMs were observed to be of moderate cytotoxicity. In vivo, cerium dioxide NMs have been reported to cause inflammatory reactions: In an acute inhalation study with rats, 15–30 nm CeO_2 nanoparticles (641 mg/m^3) increased inflammatory parameters in the BALF, including IL-1β, TNF-α, and IL-6 induction, and multifocal pulmonary microgranulomas were observed 14 days post exposure (Srinivas et al., 2011). In a STIS (Klein et al., 2012; Landsiedel et al., 2010), 0.8, 3.2, and 11.4 mg/m^3 CeO_2 NMs affected all cytological and biochemical parameters of the BALF in rats and induced IL-1α, CINC1, MCP-1, and M-CSF in BALF and lung tissue (in comparison: both CeO_2 NMs used in the present study induced TNF-α, CINC, M-CSF, and OPN). In vivo histopathology revealed diffuse histocytosis. Compared to TiO_2, CeO_2 exerted higher local irritation potential, and the effects were only partially reversible within the 3-week or 2-month observation periods (Klein et al., 2012). Evidently, the PCLuS test system used in the present study, is unable to reflect such a complex interplay of in vivo effects.

Mechanisms of action causing cytotoxicity reported for SiO_2 nanomaterials are ROS production, pro-inflammatory stimulation, protein unfolding, and membrane disruption (Damoiseaux et al., 2011; Meng et al., 2009; Napierska et al., 2010; Nel et al., 2009, 2013a). The observations made for SiO_2 NMs in the present study do not provide a uniform picture of such in vitro effects: Whereas SiO_2 NM-203 was one of the few test substances not to elicit any significant response in any of the assays, SiO_2 NM-200 activated caspase-3 and -7, which was reflected in histopathological evaluation (single cell necrosis and eosinophilic material), but did not coincide with cytotoxicity in the WST-1 assay.

In vivo short-term and subchronic inhalation studies with amorphous SiO_2 nanoparticles demonstrated largely reversible lung inflammation, granuloma formation, and focal emphysema without progressive lung fibrosis, as reviewed by Napierska et al. (2010) and Klein et al. (2012). In the rat STIS, neither precipitated SiO_2 NM-200 nor NM-203 induced any changes in the BALF or lung tissue between test substance concentrations of 0.5–10 mg/m^3 (Klein et al., 2012). In consequence, further investigations are necessary to substantiate the test results obtained for the SiO_2 NMs in the present study and to establish in vitro-in vivo correlations for SiO_2 nanomaterial effects.

Effects produced by the multi-walled carbon nanotubes. Mechanisms of action reported for MWCNT are 'frustrated phagocytosis' (i.e. stiff, non-degradable MWCNT overwhelming the phagocytic capacity of tissue macrophages thereby causing chronic tissue inflammation) and DNA oxidative injury, generation of ROS due to the metal impurities trapped inside the carbon nanotubes, pro-inflammatory effects due to oxidant injury, and pro-fibrogenic responses, and the intensitiy of these effects is reported to change with differing fiber sizes (Damoiseaux et al., 2011; Meng et al., 2009; Nel et al., 2009, 2013a,b; Rodriguez-Yanez et al., 2013).

The effects elicited by MWCNT in the present study do not provide a consistent picture of their in vitro cellular effects. MWCNT NM-400 was one of the few test substances not to elicit any significant effects in any of the assays. The other two MWCNT (NM-401 and NM-402) caused cytotoxicity at 1000 μg/mL and inflammatory reactions at non-cytotoxic concentrations (with both substances inducing CINC1 (IL-8), and NM-401 additionally inducing M-CSF, and NM-402 additionally TNF-α). Furthermore NM-401 increased GSH levels. Hence, the only pro-fibrogenic cytokine to be induced under the applied test conditions was M-CSF by MWCNT NM-401.

In vivo, MWCNTs have been observed to induce inflammatory reactions both upon acute and subchronic exposure: Rats exposed to 0.1, 0.5, or 2.5 mg/m^3 MWCNT Nanocyl® NC 7000 (equivalent to NM-400) by inhalation for 90 days developed concentration-dependent inflammatory reactions in BALF and histopathology (Ma-Hock et al., 2009b). Also in a rat STIS, 2, 8, and 32 mg/m^3 MWCNT NM-400 and MWCNT NM-402 incuded inflammatory changes in the BALF (Klein et al., 2012). In a further rat STIS investigating 0.5 and 10 mg/m^3 MWCNTs (primary structure of 15 nm outer diameter fibers, and fibrille formation at the intermediate structural range between 100 nm and 1 μm), inflammatory changes in the BALF were also observed (Ma-Hock et al., 2013). Additional investigations are necessary to specifically relate the observations made for the different MWCNTs in the PCLuS test system to specific in vivo effects.

Conclusion

With up to 120 slices to be prepared from a single rat lung, in vitro test systems making use of precision-cut lung slices could considerably reduce the numbers of animals required to detect pulmonary effects of nanomaterials as compared to in vivo studies. However, the PCLuS test protocol designed for routine testing of nanomaterials in the present study, determining cytotoxicity, caspase-3/-7 activation, glutathione reduction/increase, and cytokine induction after uniform 24-hour exposure, requires further optimization before it could come into consideration for pre-validation to assess its relevance and reliability for regulatory testing. In comparison to simple monocell culture assays, or a battery of such assays, proof-of-evidence could not yet be provided that the PCLuS possess an added value in detecting nanomaterial pulmonary toxicity.

Overall, the PCLuS test system seems susceptible to interferences with different steps of the test protocol, as observed by high variability of test substance measurements between biological replicates, high variations in the negative control measurements, and generally high negative controls (especially in the cytokine assays). The unavailability

of appropriate PC for all of the assays further stands in the way to an efficient development of the in vitro test protocols. The uniform 24-hour exposure duration prior to investigating the broad spectrum of endpoints, desirable for application of the test system for routine testing, presumably is not adequate for the caspase-3/-7, GSH, and cytokine assays. Also the option to delay test substance exposure after preparation of the tissue slices in order to better distinguish preparation-induced effects from test substance effects, should be investigated. In consequence, the results obtained in these assays should be considered preliminary.

The most robust endpoints investigated under the testing conditions of the present study assessing the effects of nanomaterials were the BCA protein and WST-1 cytotoxicity assays. These assays revealed tissue-damaging effects of the ionizing nanomaterials (ZnO and Ag) and cytotoxicity for two anatase TiO_2 NMs, both CeO_2 NMs, and one MWCNT. For the caspase-3/-7, GSH, or cytokine assays, the obtained results could not be consistently correlated to effects observed in in vivo studies. However, also other in vitro studies, making use of cell culture systems, do not yet provide consistent results allowing reliably predicting NM in vivo effects.

In summary, the present study confirms that PCLuS are able to detect different early effects of NM toxicity. Nevertheless, investigation of these effects cannot be considered sufficient to predict the much more complex and intricate apical effects that NMs might potentially induce in vivo. Furthermore, since the lung tissue burdens in the PCLuS were about three orders of magnitude higher as compared to those obtained in the STIS, any effects seen in PCLuS may not have occured in the in vivo studies. Further work is required to adjust in vitro test substance concentrations to the differing diffusion and sedimentation properties of different NMs. This is a prerequisite to ensuring that the results from different nanoform test substances obtained in different in vitro studies are comparable. Most importantly, it is a prerequisite to ensuring that the results obtained in in vitro studies can be compared to NM effects in vivo.

Conflict of interest

Some of the authors are employees of BASF SE, a company producing and marketing nanomaterials. The authors alone are responsible for the content and writing of the paper.

Acknowledgments

Appendix A. Supplementary data

Supplementary data to this article can be found online at http://dx. doi.org/10.1016/j.taap.2013.12.017.

References

Ahamed, M., Akhtar, M.J., Raja, M., Ahmad, I., Siddiqui, M.K.J., AlSalhi, M.S., Alrokayan, S.A., 2011. ZnO nanorod-induced apoptosis in human alveolar adenocarcinoma cells via p53, survivin and bax/bcl-2 pathways: role of oxidative stress. Nanomed. Nanotechnol. Biol. Med. 7 (6), 904–913.

Aitken, R.A., Bassan, A., Friedrichs, S., Hankin, S.M., Hansen, S.F., Holmqvist, J., Peters, S.A.K., Poland, C.A., Tran, C.L., 2011. Specific advice on exposure assessment and hazard/risk characterisation for nanomaterials under REACH (RIP-oN 3). Final project report. REACH-NANO consultation. RNC/RIP-oN3/FPR/1/FINAL.

Anon., 2006. Regulation (EC) No 1907/2006 of the European Parliament and of the Council of 18 December 2006 concerning the Registration, Evaluation, Authorisation and Restriction of Chemicals (REACH), establishing a European Chemicals Agency, amending Directive 1999/45/EC and repealing Council Regulation (EEC) No 793/93 and Commission Regulation (EC) No 1488/94 as well as Council Directive 76/769/EEC and Commission Directives 91/155/EEC, 93/67/EEC, 93/105/EC and 2000/21/EC (O.J. L 396/1, 30 December 2006).

Anon, 2011. Commission recommendation on the definition of nanomaterial (OJ L 275/38, 18 October 2011).

Behrsing, H.P., Furniss, M.J., Davis, M., Tomaszewski, J.E., Parchment, R.E., 2013. In vitro exposure of precision-cut lung slices to 2-(4-amino-3-methylphenyl)-5-fluorobenzothiazole lysylamide dihydrochloride (NSC 710305, Phortress) increases inflammatory cytokine content and tissue damage. Toxicol. Sci. 131 (2), 470–479.

BéruBé, K., Aufderheide, M., Breheny, D., Clothier, R., Combes, R., Duffin, R., Forbes, B., Gaça, M., Gray, A., Hall, I., Kelly, M., Lethem, M., Liebsch, M., Merolla, L., Morin, J.P., Seagrave, J., Swartz, M.A., Tetley, T.D., Umachandran, M., 2009. In vitro models of inhalation toxicity and disease. The report of a FRAME workshop. Altern. Lab. Anim. 37 (1), 89–141.

Cho, W.S., Duffin, R., Poland, C.A., Howie, S.E., MacNee, W., Bradley, M., Megson, I.L., Donaldson, K., 2010. Metal oxide nanoparticles induce unique inflammatory footprints in the lung: important implications for nanoparticle testing. Environ. Health Perspect. 118 (12), 1699–1706.

Damoiseaux, R., George, S., Li, M., Pokhrel, S., Ji, Z., France, B., Xia, T., Suarez, E., Rallo, R., Mädler, L., Cohen, Y., Hoek, E.M.V., Nel, A.E., 2011. No time to lose–high throughput screening to assess nanomaterial safety. Nanoscale 3 (4), 1345–1360.

Donaldson, K., Borm, P.J., Oberdörster, G., Pinkerton, K.E., Stone, V., Tran, C.L., 2008. Concordance between in vitro and in vivo dosimetry in the proinflammatory effects of low-toxicity, low-solubility particles: the key role of the proximal alveolar region. Inhal. Toxicol. 20 (1), 53–62.

Donaldson, K., Murphy, F.A., Duffin, R., Poland, C.A., 2010. Asbestos, carbon nanotubes and the pleural mesothelium: a review of the hypothesis regarding the role of long fibre retention in the parietal pleura, inflammation and mesothelioma. Part. Fibre Toxicol. 22 (7), 5.

Duffin, R., Mills, N.L., Donaldson, K., 2007a. Nanoparticles — a thoracic toxicology perspective. Yonsei Med. J. 48 (4), 561–572.

Duffin, R., Tran, L., Brown, D., Stone, V., Donaldson, K., 2007b. Proinflammogenic effects of low-toxicity and metal nanoparticles in vivo and in vitro: highlighting the role of particle surface area and surface reactivity. Inhal. Toxicol. 19 (10), 849–856.

Feltis, B.N., O'Keefe, S.J., Harford, A.J., Piva, T.J., Turney, T.W., Wright, P.F.A., 2012. Independent cytotoxic and inflammatory responses to zinc oxide nanoparticles in human monocytes and macrophages. Nanotoxicology 6 (7), 757–765.

Fentem, J.H., Prinsen, M.K., Spielmann, H., Walum, E., Botham, P.A., 1995. Validation — lessons learned from practical experience. Toxicol. In Vitro 9 (6), 857–862.

Gasser, M., Wick, P., Clift, M.J., Blank, F., Diener, L., Yan, B., Gehr, P., Krug, H.F., Rothen-Rutishauser, B., 2012. Pulmonary surfactant coating of multi-walled carbon nanotubes (MWCNTs) influences their oxidative and pro-inflammatory potential in vitro. Part. Fibre Toxicol. 9 (1), 17.

Gojova, A., Guo, B., Kota, R.S., Rutledge, J.C., Kennedy, I.M., Barakat, A.I., 2007. Induction of inflammation in vascular endothelial cells by metal oxide nanoparticles: effect of particle composition. Environ. Health Perspect. 115, 403–409.

Guadagnini, R., Halamoda Kenzaoui, B., Cartwright, L., Pojana, G., Magdolenova, Z., Bilanicova, D., Saunders, M., Juillerat, L., Marcomini, A., Huk, A., Dusinska, M., Fjellsbø, L.M., Marano, F., Boland, S., 2013. Toxicity screenings of nanomaterials: challenges due to interference with assay processes and components of classic in vitro tests. Nanotoxicology. http://dx.doi.org/10.3109/17435390.2013.829590 (2013/Jul, epub ahead of print).

Hackenberg, S., Scherzed, A., Technau, A., Kessler, M., Froelich, K., Ginzkey, C., Koehler, C., Burghartz, M., Hagen, R., Kleinsasser, N., 2011. Cytotoxic, genotoxic and pro-inflammatory effects of zinc oxide nanoparticles in human nasal mucosa cells in vitro. Toxicol. In Vitro 25, 657–663.

Hankin, S.M., Peters, S.A.K., Poland, C.A., Foss Hansen, S., Holmqvist, J., Ross, B.L., Varet, J., Aitken, R.J., 2011. Specific advice on fulfilling information requirements for nanomaterials under REACH (RIP-oN 2). Final project report. REACH-NANO consultation. RNC/RIP-oN2/FPR/1/FINAL (available at: http://ec.europa.eu/environment/chemicals/nanotech/pdf/report_riponn2.pdf).

Heng, B.C., Zhao, X., Tan, E.C., Khamis, N., Assodani, A., Xiong, S., Ruedl, C., Ng, K.W., Loo, J.S.-C., 2011a. Evaluation of the cytotoxic and inflammatory potential of differentially shaped zinc oxide nanoparticles. Arch. Toxicol. 85, 1517–1528.

Heng, B.C., Zhao, X., Xiong, S., Ng, K.W., Boey, F.Y.C., Loo, J.S.C., 2011b. Cytotoxicity of zinc oxide (ZnO) nanoparticles is influenced by cell density and culture format. Arch. Toxicol. 85, 695–704.

Henjakovic, M., Martin, C., Hoymann, H.G., Sewald, K., Ressmeyer, A.R., Dassow, C., Pohlmann, G., Krug, N., Uhlig, S., Braun, A., 2008. Ex vivo lung function measurements in precision-cut lung slices (PCLS) from chemical allergen-sensitized mice represent a suitable alternative to in vivo studies. Toxicol. Sci. 106 (2), 444–453.

Herzog, F., Clift, M.J.D., Piccapietra, F., Behra, R., Schmid, O., Petri-Fink, A., Rothen-Rutishauser, B., 2013. Exposure of silver-nanoparticles and silver ions to lung cells in vitro at the air liquid interface. Part. Fibre Toxicol. 10, 11.

Himi, T., Yoshioka, I., Kataura, A., 1997. Production and gene expression of IL-8-like cytokine GRO/CINC-1 in rat nasal mucosa. Acta Otolaryngol. 117 (1), 123–127.

Hinderliter, P.M., Minard, K.R., Orr, G., Chrisler, W.B., Thrall, B.D., Pounds, J.G., Teeguarden, J.G., 2010. ISDD: A computational model of particle sedimentation, diffusion and target cell dosimetry for in vitro toxicity studies. Part. Fibre Toxicol. 7 (1), 36.

Hirsch, C., Roesslein, M., Krug, H.F., Wick, P., 2011. Nanomaterial cell interactions: are current in vitro tests reliable? Nanomedicine 6 (5), 837–847.

Horev-Azaria, L., Kirkpatrick, C.J., Korenstein, R., Marche, P.N., Maimon, O., Ponti, J., Romano, R., Rossi, F., Golla-Schindler, U., Sommer, D., Uboldi, C., Unger, R.E., Villiers,

C., 2011. Predictive toxicology of cobalt nanoparticles and ions: comparative in vitro study of different cellular models using methods of knowledge discovery from data. Toxicol. Sci. 122 (2), 489–501.

Hussain, S., Thomassen, L.C.J., Ferecatu, I., Borot, M.C., Andreau, K., Martens, J.A., Fleury, J., Baeza-Squiban, A., Marano, F., Boland, S., 2010. Carbon black and titanium dioxide nanoparticles elicit distinct apoptotic pathways in bronchial epithelial cells. Part. Fibre Toxicol. 7, 10.

ICRP (International Commission on Radiological Protection), 1994. ICRP Publication No. 66: Human respiratory tract model for radiological protection. Ann. ICRP 24, 1–3.

Janardhan, K.S., McIsaac, M., Fowlie, J., Shrivastav, A., Caldwell, S., Sharma, R.K., Singh, B., 2006. Toll like receptor-4 expression in lipopolysaccharide induced lung inflammation. Histol. Histopathol. 21 (7), 687–696.

Johnston, H.J., Hutchison, G.R., Christensen, F.M., Peters, S., Hankin, S., Stone, V., 2009. Identification of the mechanisms that drive the toxicity of TiO_2 particulates: the contribution of physicochemical characteristics. Part. Fibre Toxicol. 6, 33.

Johnston, H.J., Hutchison, G.R., Christensen, F.M., Peters, S., Hankin, S., Stone, V., 2010. A review of the in vivo and in vitro toxicity of silver and gold particulates: particle attributes and biological mechanisms responsible for the observed toxicity. Crit. Rev. Toxicol. 40 (4), 328–346.

Kao, Y.-Y., Chen, Y.-C., Cheng, T.-J., Chiung, Y.-M., Liu, P.-S., 2012. Zinc oxide nanoparticles interfere with zinc ion homeostasis to cause cytotoxicity. Toxicol. Sci. 125 (2), 462–472.

Kermanizadeh, A., Pojana, G., Gaiser, B.K., Birkedal, R., Bilaničová, D., Wallin, H., Jensen, K.A., Sellergren, B., Hutchison, G.R., Marcomini, A., Stone, V., 2013. In vitro assessment of engineered nanomaterials using a hepatocyte cell line: cytotoxicity, pro-inflammatory cytokines and functional markers. Nanotoxicology 7 (3), 301–313.

Klein, C.L., Wiench, K., Wiemann, M., Ma-Hock, L., van Ravenzwaay, B., Landsiedel, R., 2012. Hazard identification of inhaled nanomaterials: making use of short-term inhalation studies. Arch. Toxicol. 86 (7), 1137–1151.

Kotchey, G.P., Gaugler, J.A., Kapralov, A.A., Kagan, V.E., Star, A., 2013. Effect of antioxidants on enzyme-catalysed biodegradation of carbon nanotubes. J. Mater. Chem. B Mater. Biol. Med. 1 (3), 302–309.

Kroll, A., Dierker, C., Rommel, C., Hahn, D., Wohlleben, W., Schulze-Isfort, C., Göbbert, C., Voetz, M., Hardinghaus, F., Schnekenburger, J., 2011. Cytotoxicity screening of 23 engineered nanomaterials using a test matrix of ten cell lines and three different assays. Part. Fibre Toxicol. 8, 9.

Kuempel, E.D., Castranova, V., Geraci, C.L., Schulte, P.A., 2012. Development of risk-based nanomaterial groups for occupational exposure control. J. Nanopart. Res. 14, 1029.

Lamkanfi, M., 2011. Emerging inflammasome effector mechanisms. Nat. Rev. Immunol. 11 (3), 213–220.

Landsiedel, R., Ma-Hock, L., Kroll, A., Hahn, D., Schnekenburger, J., Wiench, K., Wohlleben, W., 2010. Testing metal-oxide nanomaterials for human safety. Adv. Mater. 22, 2601–2627.

Landsiedel, R., Ma-Hock, L., Haussmann, H.J., van Ravenzwaay, B., Kayser, M., Wiench, K., 2012. Inhalation studies for the safety assessment of nanomaterials: status quo and the way forward. Wiley Interdiscip. Rev. Nanomed. Nanobiotechnol. 4 (4), 399–413.

Lauenstein, L., Hess, A., Vogel, S., Schneider, X., Martin, C., Pirow, R., Liebsch, M., Landsiedel, R., Braun, A., Sewald, K., 2012. Pre-validation of the PCLS ex vivo model for the prediction of respiratory toxicity. ATLA 40 (4), A18.

Lin, T., Yang, M.S., 2007. Benzo[a]pyrene-induced elevation of GSH level protects against oxidative stress and enhances xenobiotic detoxification in human HepG2 cells. Toxicology 235 (1–2), 1–10.

Lorne, E., Dupont, H., Abraham, E., 2010. Toll-like receptors 2 and 4: initiators of non-septic inflammation in critical care medicine? Intensive Care Med. 36 (11), 1826–1835.

Lupu, A.R., Popescu, T., 2013. The noncellular reduction of MTT tetrazolium salt by TiO_2 nanoparticles and its implications for cytotoxicity assays. Toxicol. In Vitro 27 (5), 1445–1450.

Ma-Hock, L., Burkhardt, S., Strauss, V., Gamer, A.O., Wiench, K., van Ravenzwaay, B., Landsiedel, R., 2009a. Development of a short-term inhalation test in the rat using nano-titanium dioxide as a model substance. Inhal. Toxicol. 21 (2), 102–118.

Ma-Hock, L., Treumann, S., Strauss, V., Brill, S., Luizi, F., Mertler, M., Wiench, K., Gamer, A.O., van Ravenzwaay, B., Landsiedel, R., 2009b. Inhalation toxicity of multiwall carbon nanotubes in rats exposed for 3 months. Toxicol. Sci. 112 (2), 468–481.

Ma-Hock, L., Strauss, V., Treumann, S., Küttler, K., Wohlleben, W., Hofmann, T., Gröters, S., Wiench, K., van Ravenzwaay, B., Landsiedel, R., 2013. Comparative inhalation toxicity of multi-wall carbon nanotubes, graphene, graphite nanoplatelets and low surface carbon black. Part. Fibre Toxicol. 10 (1), 23.

Martin, C., Uhlig, S., Ullrich, V., 1996. Videomicroscopy of methacholine-induced contraction of individual airways in precision- cut lung slices. Eur. Respir. J. 9 (12), 2479–2487.

Martin, C., Held, H.D., Uhlig, S., 2000. Differential effects of the mixed ET(A)/ET(B)-receptor antagonist bosentan on endothelin-induced bronchoconstriction, vasoconstriction and prostacyclin release. Naunyn Schmiedebergs Arch. Pharmacol. 362 (2), 128–136.

McComb, S., Mulligan, R., Sad, S., 2010. Caspase-3 is transiently activated without cell death during early antigen driven expasion of CD8+ T cells in vivo. PLoS One 5 (12), e15328.

Meng, H., Xia, T., George, S., Nel, A.E., 2009. A predictive toxicological paradigm for the safety assessment of nanomaterials. ACS Nano 3 (7), 1620–1627.

Monopoli, M.P., Walczyk, D., Campbell, A., Elia, G., Lynch, I., Bombelli, F.B., Dawson, K.A., 2011. Physical–chemical aspects of protein corona: relevance to in vitro and in vivo biological impacts of nanoparticles. J. Am. Chem. Soc. 133 (8), 2525–2534.

Monopoli, M.P., Åberg, C., Salvati, A., Dawson, K.A., 2012. Biomolecular coronas provide the biological identity of nanosized materials. Nat. Nanotechnol. 7, 779–786.

Monteiller, C., Tran, L., MacNee, W., Faux, S.P., Jones, A., Miller, B., Donaldson, K., 2007. The pro-inflammatory effects of low-toxicity low-solubility particles, nanoparticles and fine particles, on epithelial cells in vitro: The role of surface area. Occup. Environ. Med. 64, 609–615.

Müller, L., Riediker, M., Wick, P., Mohr, M., Gehr, P., Rothen-Rutishauser, B., 2010. Oxidative stress and inflammation response after nanoparticle exposure: differences between human lung cell monocultures and an advanced three-dimensional model of the human epithelial airways. J. R. Soc. Interface 7, S27–S40.

Murdock, R.C., Braydich-Stolle, L., Schrand, A.M., Schlager, J.J., Hussain, S.M., 2008. Characterization of nanomaterial dispersion in solution prior to in vitro exposure using dynamic light scattering technique. Toxicol. Sci. 101 (2), 239–253.

Napierska, D., Thomassen, L.C., Lison, D., Martens, J.A., Hoet, P.H., 2010. The nanosilica hazard: another variable entity. Part. Fibre Toxicol. 7 (1), 39.

Nassimi, M., Schleh, C., Lauenstein, H.-D., Hussein, R., Lübbers, K., Pohlmann, G., Switalla, S., Sewald, K., Müller, M., Krug, N., Müller-Goymann, C.C., Braun, A., 2009. Low cytotoxicity of solid lipid nanoparticles in in vitro and ex vivo lung models. Inhal. Toxicol. 21, 104–109.

Nel, A.E., Mädler, L., Velegol, D., Xia, T., Hoek, E.M.V., Somasundaran, P., Klaessig, F., Castranova, V., Thompson, M., 2009. Understanding biophysicochemical interactions at the nano-bio interface. Nat. Mater. 8 (7), 543–557.

Nel, A.E., Xia, T., Meng, H., Wang, X., Lin, S., Ji, Z., Zhang, H., 2013a. Nanomaterial toxicity testing in the 21st century: use of a predictive toxicological approach and high-throughput screening. Acc. Chem. Res. 46 (3), 607–621.

Nel, A.E., Nasser, E., Godwin, H., Avery, D., Bahadori, T., Bergeson, L., Beryt, E., Bonner, J.C., Boverhof, D., Carter, J., Castranova, V., Deshazo, J.R., Hussain, S.M., Kane, A.B., Klaessig, F., Kuempel, E., Lafranconi, M., Landsiedel, R., Malloy, T., Miller, M.B., Morris, J., Moss, K., Oberdorster, G., Pinkerton, K., Pleus, R.C., Shatkin, J.A., Thomas, R., Tolaymat, T., Wang, A., Wong, J., 2013b. A multi-stakeholder perspective on the use of alternative test strategies for nanomaterial safety assessment. ACS Nano 7 (8), 6422–6433.

Oberdörster, G., 2009. Safety assessment for nanotechnology and nanomedicine: concepts of nanotoxicology. J. Int. Med. 267 (1), 89–105.

Oberdörster, G., Ferin, J., Lehnert, B.E., 1994. Correlation between particle size, in vivo particle persistence, and lung injury. Environ. Health Perspect. 102 (Suppl. 5), 173–179.

OECD, 2008. List of manufactured nanomaterials and list of endpoints for phase one of the OECD testing programme. Series on the safety of manufactured nanomaterials, number 6.OECD, Paris (ENV/JM/MONO(2008)13/REV, 7 July 2008).

OECD, 2009. OECD guideline for the testing of chemicals. Acute inhalation toxicity. (Adopted: 7 September 2009).

OECD, 2010. Guidance manual for the testing of manufactured nanomaterials: OECD's sponsorship programme; first revision. OECD, Paris (ENV-JM-MONO(2009)20-REV, 2 June 2010).

Okamura, K., Dummer, P., Kopp, J., Qiu, L., Levi, M., Faubel, S., Blaine, J., 2013. Endocytosis of albumin by podocytes elicits an inflammatory response and induces apoptotic cell death. PLoS One 8 (1), e54817.

Park, E.-J., Yi, J., Chung, K.-H., Ryu, D.-Y., Choi, J., Park, K., 2008. Oxidative stress and apoptosis induced by titanium dioxide nanoparticles in cultured BEAS-2B cells. Toxicol. Lett. 180, 222–229.

Pastore, A., Federici, G., Bertini, E., Piemonte, F., 2003. Analysis of glutathione: implication in redox and detoxification. Clin. Chim. Acta 333 (1), 19–39.

Peskin, A.V., Winterbourn, C.C., 2000). A microtiter plate assay for superoxide dismutase using a water-soluble tetrazolium salt (WST-1). Clin. Chim. Acta 293 (1–2), 157–166.

Rodriguez-Yanez, Y., Munoz, B., Albores, A., 2013. Mechanisms of toxicity by carbon nanotubes. Toxicol. Mech. Methods 23 (3), 178–195.

Rothen-Rutishauser, B.M., Kiama, S.G., Gehr, P., 2005. A three-dimensional cellular model of the human respiratory tract to study the interaction with particles. Am. J. Respir. Cell Mol. Biol. 32, 281–289.

Roy, R., Tripathi, A., Das, M., Dwivedi, P.D., 2011. Cytotoxicity and uptake of zinc oxide nanoparticles leading to enhanced inflammatory cytokines levels in murine macrophages: comparison with bulk zinc oxide. J. Biomed. Nanotechnol. 7, 110–111.

Rushton, E.K., Jiang, J., Leonard, S.S., Eberly, S., Castranova, V., Biswas, P., Elder, A., Han, X., Gelein, R., Finkelstein, J., Oberdörster, G., 2010. Concept of assessing nanoparticle hazards considering nanoparticle dosemetric and chemical/biological response metrics. J. Toxicol. Environ. Health A 73 (5), 445–461.

Saito, T., Yamamoto, T., Kazawa, T., Gejyo, H., Naito, M., 2005. Expression of toll-like receptor 2 and 4 in lipopolysaccharide-induced lung injury in mouse. Cell Tissue Res. 321 (1), 75–88.

Schaefer, J., Schulze, C., Marxer, E.E., Schaefer, U.F., Wohlleben, W., Bakowsky, U., Lehr, C.M., 2012. Atomic force microscopy and analytical ultracentrifugation for probing nanomaterial protein interactions. ACS Nano 6 (6), 4603–4614.

Schroder, K., Tschopp, J., 2010. The inflammasomes. Cell 140, 821–832.

Seiffert, J.M., Baradez, M.-O., Nischwitz, V., Lekishvili, T., Goenaga-Infante, H., Marshall, D., 2012. Dynamic monitoring of metal oxide nanoparticle toxicity by label free impedance sensing. Chem. Res. Toxicol. 25 (1), 140–152.

Shvedova, A.A., Pietroiusti, A., Fadeel, B., Kagan, V.E., 2012. Mechanisms of carbon nanotube-induced toxicity: focus on oxidative stress. Toxicol. Appl. Pharmacol. 261 (2), 121–133.

Singh, C., Friedrichs, S., Levin, M., Birkedal, R., Jensen, K.A., Pojana, G., Wohlleben, W., Schulte, S., Wiench, K., Turney, T., Koulaeva, O., Marshall, D., Hund-Rinke, K., Kördel, W., van Doren, E., de Temmerman, P.-J., Abi Daoud Francisco, M., Mast, J., Gibson, N., Koeber, R., Linsinger, T., Klein, C.L., 2011. NM series of representative manufactured nanomaterials. Zinc oxide NM-110, NM-111, NM-112, NM-113 characterisation and test item preparation. European Commission, Joint Research Centre, Institute for Reference Materials and Measurements (141 pp.).

Slee, E.A., Adrain, C., Martin, S.J., 2001. Executioner caspase-3, -6, and -7 perform distinct, non-redundant roles during the demolition phase of apoptosis. J. Biol. Chem. 276, 7320–7326.

Song, K.S., Sung, J.H., Ji, J.H., Lee, J.H., Lee, J.S., Ryu, H.R., Lee, J.K., Chung, Y.H., Park, H.M., Shin, B.S., Chang, H.K., Kelman, B., Yu, I.J., 2013. Recovery from silver-nanoparticle-exposure-induced lung inflammation and lung function changes in Sprague Dawley rats. Nanotoxicology 7 (2), 169–180.

Srinivas, A., Rao, P.J., Selvam, G., Murthy, P.B., Reddy, P.N., 2011. Acute inhalation toxicity of cerium oxide nanoparticles in rats. Toxicol. Lett. 205 (2), 105–115.

Stone, V., Johnston, H., Schins, R.P.F., 2009. Development of in vitro systems for nanotoxicology: methodological considerations. Crit. Rev. Toxicol. 39 (7), 613–626.

Sung, J.H., Ji, J.H., Park, J.D., Yoon, J.U., Kim, D.S., Jeon, K.S., Song, M.Y., Jeong, J., Han, B.S., Han, J.H., Chung, Y.H., Chang, H.K., Lee, J.H., Cho, M.H., Kelman, B.J., Yu, I.J., 2009. Subchronic inhalation toxicity of silver nanoparticles. Toxicol. Sci. 108 (2), 452–461.

Sung, J.H., Ji, J.H., Song, K.S., Lee, J.H., Choi, K.H., Lee, S.H., Yu, I.J., 2011. Acute inhalation toxicity of silver nanoparticles. Toxicol. Ind. Health 27 (2), 149–154.

Switalla, S., Knebel, J., Ritter, D., Krug, N., Braun, A., Sewald, K., 2010a. Effects of acute in vitro exposure of murine precision-cut lung slices to gaseous nitrogen dioxide and ozone in an air liquid interface (ALI) culture. Toxicol. Lett. 196 (2), 117–124.

Switalla, S., Lauenstein, L., Prenzler, F., Knothe, S., Förster, C., Fieguth, H.G., Pfennig, O., Schaumann, F., Martin, C., Guzman, C.A., Ebensen, T., Müller, M., Hohlfeld, J.M., Krug, N., Braun, A., Sewald, K., 2010b. Natural innate cytokine response to immuno-modulators and adjuvants in human precision-cut lung slices. Toxicol. Appl. Pharmacol. 246 (3), 107–115.

Teeguarden, J.G., Hinderliter, P.M., Orr, G., Thrall, B.D., Pounds, J.G., 2007. Particokinetics in vitro: dosimetry considerations for in vitro nanoparticle toxicity assessments. Toxicol. Sci. 95 (2), 300–312 (erratum in: Toxicol. Sci., 2007. 97(2), 614).

van Ravenzwaay, B., Landsiedel, R., Fabian, E., Burkhardt, S., Strauss, V., Ma-Hock, L., 2009. Comparing fate and effects of three particles of different surface properties: nano-TiO$_2$, pigmentary TiO$_2$ and quartz. Toxicol. Lett. 186, 152–159.

Wilhelmi, V., Fischer, U., van Berlo, D., Schulze-Osthoff, K., Schins, R.P.F., Albrecht, C., 2012. Evaluation of apoptosis induced by nanoparticles and fine particles in RAW 264.7 macrophages: facts and artefacts. Toxicol. In Vitro 26 (2), 323–334.

Wohlleben, W., 2012. Validity range of centrifuges for the regulation of nanomaterials: from classification to as-tested coronas. J. Nanopart. Res. 14 (12), 1300.

Wohlleben, W., Kolle, S.N., Hasenkamp, L.C., Böser, A., Vogel, S., von Vacano, B., van Ravenzwaay, B., Landsiedel, R., 2011. Artifacts by marker enzyme adsorption on nanomaterials in cytotoxicity assays with tissue cultures. J. Phys. Conf. Ser. 304. http://dx.doi.org/10.1088/1742-6596/304/1/012061.

Wohlsen, A., Martin, C., Vollmer, E., Branscheid, D., Magnussen, H., Becker, W.M., Lepp, U., Uhlig, S., 2003. The early allergic response in small airways of human precision-cut lung slices. Eur. Respir. J. 21, 1024–1032.

Xia, T., Kovochich, M., Liong, M., Madler, L., Gilbert, B., Shi, H., Yeh, J.I., Zink, J.I., Nel, A.E., 2008. Comparison of the mechanism of toxicity of zinc oxide and cerium oxide nanoparticles based on dissolution and oxidative stress properties. ACS Nano 2, 2121–2134.

Zhu, M., Nie, G., Meng, H., Xia, T., Nel, A., Zhao, Y., 2013. Physicochemical properties determine nanomaterial cellular uptake, transport and fate. Acc. Chem. Res. 46 (3), 622–631.